Microthrombosis Induced by Mechanical Factors and Light-dye Treatment in Intact Microvessels

by

Qin Liu

A dissertation submitted to the Graduate Faculty in Biomedical Engineering in partial fulfillment of the requirements for the degree of Doctor of Philosophy, The City University of New York

2010

This manuscript has been read and accepted for the Graduate Faculty in Biomedical Engineering in satisfaction of the dissertation requirement for the degree of Doctor of Philosophy.

Professor Bingmei M. Fu

Date

Chair of Examining Committee

Professor Mumtaz Kassir

Date

Executive Officer

Professor John M. Tarbell

Professor Sihong Wang

Professor Peter Ganatos

Professor Qianhong Wu

Supervision Committee

THE CITY UNIVERSITY OF NEW YORK

ABSTRACT

MICROTHROMBOSIS INDUCED BY MECHANICAL FACTORS AND LIGHT-DYE TREATMENT IN INTACT MICROVESSELS

by

Qin Liu

Advisor: Dr. Bingmei M. Fu

Thrombosis is the formation of a blood clot in a blood vessel. When thrombosis happens in the brain, it would cause stroke; when happens in the heart, it would cause heart attack. If a thrombus travels to the lung, it would cause pulmonary embolism and lead to death under certain circumstances. Although both chemical and mechanical factors can induce thrombosis, the quantitative understanding of the contribution from mechanical factors is poor, especially in the microvasculature with non-disturbed laminar flows. The first part of this study thus investigated the relation between localized shear rates/stresses and thrombosis in bent microvessels with low Reynolds number blood flows. *In vivo* experiments on microvessels in rat mesentery revealed that thrombi were initiated at the inner wall of the bent vessel, while computational results demonstrated that there was a higher shear stress/rate and a higher shear stress/rate gradient at the inner wall of the bent vessel, which could activate endothelial and blood cells for binding. These results suggest that the higher shear stress/rate and the higher shear stress/rate gradient are the mechanical factors inducing thrombi in the microvessels with very low Reynolds number flows.

Photodynamic therapy (PDT) is a treatment that uses a photosensitizer (photosensitizing agent) excited by a specific wavelength light to treat various diseases including tumors. However, PDT also induces thrombosis in the blood vessels of normal tissues adjacent to the tumor. To search for a preventive method for unwanted thrombosis, in the second part of the study, we examined the structural mechanisms by which light/dye treatment induces microvascular hyperpermeability and thrombosis. *In vivo* experiments showed that under the similar light/dye treatment, microvessel thrombosis and hyperpermeability were highly correlated with each other. Comparison of the measured permeability data with predictions from a mathematical model for the inter-endothelial cleft suggests that an almost complete depletion of the glycocalyx layer at the luminal surface of the endothelium is the most likely structural mechanism by which the light/dye increases microvascular permeability and induces thrombosis. If the light/dye degrades the surface glycocalyx to increase vessel permeability, the increased radial fluid flow across the microvessel wall would bring platelets and leukocytes closer to the proximity of the wall and enhance the opportunity of their binding to endothelium. In addition, removing the surface glycocalyx would expose endothelium for the binding.

ACKNOWLEDGEMENTS

I would like to give my thanks to my supervisor, Professor Bingmei M. Fu, for her support, encouragement and advice, for providing me with an environment allowing me to do research independently, for her leading me into the challenging field of research and for always helping to build the foundation of my future career. Her positive attitude with which she approaches any challenge has always been inspirational. It has not always been an easy road, but she has been an anchor of support throughout my research.

I would also like to give my thanks to the members of my thesis committee: Professor John Tarbell (CCNY), Professor Sihong Wang (CCNY), Professor Peter Ganatos (CCNY), and Professor Qianhong Wu (Villanova University). They have been a source of encouragement and advice that have contributed a great deal in the course of my Ph.D. work. I would also thank Professor Jeffery Morris (CCNY) for his guidance and help in my work.

I would like to give my special thanks to my colleagues, Dr. Min Zeng, Bin Cai, Wei Yuan, Guanglei Li, and Jie Fan. They gave me tremendous help and support, and this project could not exist without any of them.

Lastly, I would like to thank my family for their unconditional love and support throughout the years.

CONTENTS

LIST OF TABLES

LIST OF FIGURES

CHAPTER 1 INTRODUCTION

Thrombosis

Thrombosis is the formation of a clot in a blood vessel, which obstructs the blood flow in the circulation. There are two types of thrombi, venous thrombi and arterial thrombi. A major type of venous thrombi occurs in the deep vein of the leg (DVT, deep vein thrombus) where the vein is damaged or the flow slows down or stops. This type of thrombi consists of red blood cells and fibrin (red thrombus) (Grabowski *et al.*, 1995). Although many thrombi are small and do not cause serious problems, some of them can be fatal. For example, if the DVT partially or completely blocks the blood flow through the vessel, blood begins to pool and may develop swelling and pain. If a large thrombus in the vein breaks and travels to the lung, it can cause pulmonary embolism (PE), which may lead to death. Another type of thrombi, arterial thrombi, mainly consists of platelets and fibrin. Since they lack of red blood cells, they are often called white thrombi. Arterial thrombi occurring in coronary arteries would lead to heart attack. Micro-thrombi in arterioles consist of platelets only, and those in venules consist of platelets and a few leukocytes (Rumbaut *et al.*, 2005).

Classical theory (Hume *et al.*, 1970) presented three possible causes of venous thrombosis: 1) a primary lesion in the endothelium, which produces an inflammatory reaction and then thrombosis; 2) a slowed or other abnormal flow resulting in the adhesion of blood cells and blood-borne elements to the vessel wall, which leads to

thrombosis; and 3) increase of blood coagulability from changes in the physical and/or chemical properties of plasma. Venous thrombi may develop by one or the combination of any of these factors. For example, if there is a lesion, i.e., an opening of gaps between endothelial cells, invoked by local factors in the endothelium, platelets will adhere in these gaps where basement membrane is exposed and a thrombus will form. Wessler *et al.* (1962) found that venous thrombi may be developed by the combination of vascular stasis and altered coagulability of the blood without intimal damage.

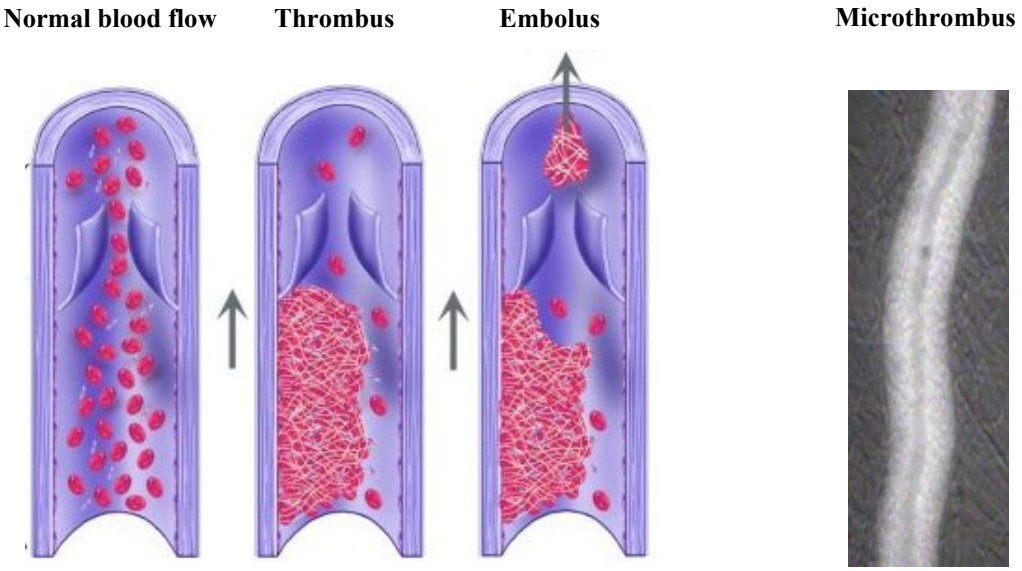

Fig. 1.1 Thrombosis in vessels. (a) In large vessels (from http://www.daviddarling.info/encyclopedia/D/deep_vein_thrombosis.html); (b) in a post-capillary venule of rat mesentery.

Thrombosis induced by mechanical factors

Both mechanical and chemical factors can affect the activity of platelet coagulation factors responsible for the formation of thrombus near an injured/damaged vessel. However it has been found that physical factors alone, without exogenous chemical factors, can induce platelet aggregation. O'Brien (1990) found shear stress alone induced platelet aggregation in a manner similar to that observed on an injured vessel wall. Experiments of blood flowing through a capillary tube showed that a local hemostatic plug formed after a small hole was produced on a tube wall, suggesting physical forces and geometric changes can induce thrombosis without addition of chemical agonists (Muga *et al.*, 1995). Previous studies proposed that the physical factors responsible for thrombosis are magnitudes of shear stress/rate, local geometry of the vessel, and the duration of the applied physical forces (Grabowski, 1995; Noren *et al.*, 2000; Turitto *et al.*, 1998). The endothelial cells can become antithrombotic or prothrombotic depending on the magnitude and duration of the shear forces applied. In the regions of irregular geometry, such as at branches or stenoses, flow streamlines are altered by the irregular geometry and induce localized shear stresses/rates, which may induce accumulation of blood cells at the specific regions. A recirculation zone may form depending on the magnitude of Reynolds number of the flow and the geometry of the stenoses. Low shear condition and long residence time would favor this formation (Turitto *et al.*, 1998). Endothelial cells may also become prothrombotic at certain magnitudes of shear stresses/rates, leading to platelet aggregation and fibrin formation (Grabowski, 1995; Noren *et al.*,

2000). Studies (Sato *et al.*, 1990) on microvessels (arterioles/venules) of rat mesentery showed that thrombi initiation depended significantly on shear rate rather than the flow velocity. In their experiments, the microvessels were injured using irradiation method. It was observed that thrombi were initiated at locations of higher shear rates in venules and lower shear rates in arterioles. The relation between thrombi initiation time and shear rate was almost linear. However, all above previous studies on thrombosis were conducted under the conditions either the flow was retarded (Nicolaides *et al.*, 1972; Wessler, 1962) or disturbed (secondary flow) (Chen and Lu, 2004; Wootton and Ku, 1999), or the vessels were injured/damaged by using various electrical, chemical and physical methods (summarized by Rumbaut *et al.*, 2005).

Thrombosis induced by light/dye treatment

Photodynamic Therapy (PDT) is a minimally invasive modality in which a photosensitizer is applied and activated by a laser at a specific wavelength in the presence of oxygen, leading to cellular and tissue effects. Light therapy was used 3000 years ago (Daniell *et al.*, 1991), but the modern era of PDT started with the studies of Lipson and Schwartz at the Mayo Clinic in 1960. They developed a compound called "haematoporphyrin derivative" (HPD) and found it was localized to the tumor when excited under the laser. That HPD selectively accumulates in tumor was assumed due to its high vascular permeability and its affinity to proliferating endothelium, and the lack of lymphatic drainage in tumors (Dougherty *et al.*, 1998). Unlike radiation therapy or surgery, PDT can be applied repeatedly at the same site.

This treatment is also selective because the photosensitizer can selectively accumulate in the tumor cells, and it is harmless without light illumination. The treatment occurs only in the illuminated area and only during illumination. The patient does not undergo needless systemic treatment when treating localized diseases. This allows a better therapeutic control and a significant reduction of side effects. In addition, PDT can treat diseases that surgery is not possible, e.g., a cancer in structure that cannot be removed surgically (such as in upper bronchi of the lung). Because of these advantages, PDT is used in the treatment for various types of cancers, including lung, skin, gastrointestinal tract, brain, head and neck, bladder, and pancreatic cancers (Dolmans *et al.*, 2003). It has also been used in treating age-related macular degeneration (AMD), ophthalmology, cardiovascular diseases, actinic keratosis, and rheumatology (Dougherty, 2002; Detty *et al.*, 2004).

In general, the effect of PDT depends on the type, dose, and location (extracellular or intracellular) of photosensitizer, the light intensity and length of the exposure time, the availability of oxygen, and the interval between the photosensitizer administration and light exposure (Stylli *et al.*, 2006). The mechanisms by which PDT induces tumor destruction include direct tumor cell killing, immune reaction, and vascular damage (Ortner *et al.*, 2006). When the photosensitizer is activated by the light, it transfers energy from light to molecular oxygen to produce reactive oxygen species (ROS). These free radicals would damage the endothelial and vascular basement membrane, leading to thrombosis. By inhibiting free radical production, thrombosis was inhibited (Giuseppe *et al.*, 2004). This form of oxygen

(free radical) is cytotoxic, with a short lifetime and a short radius of action; therefore only cells close to it are affected by PDT (Dolmans *et al.*, 2003). Although vascular damage has long been known to be induced by PDT, intentional use of this mechanism only began recently, starting with the treatment of AMD (Michels *et al.*, 2003). The immediate response after PDT was vasoconstriction, and the increase in vascular permeability. The long-term response was thrombus formation, occlusion of the vessel and vascular shutdown (Michels *et al.*, 2003; Chen *et al.*, 2006). Experiments on big blood vessels and nerves in rabbits (Kübler *et al.*, 2003) showed that severe edema, media-hyperplasia or thrombosis occurred in the vessels during intra-operative PDT. Although PDT induced thrombosis is important for successful treatment of tumors, PDT would also cause unwanted thrombosis in normal vessels of tissues adjacent to the tumor.

Light/dye treatment, similar to PDT, is the use of a fluorescent dye administrated systemically and exposure to a light with the matching wavelength. Rosenblum *et al.* (1977) first reported the application of light and sodium fluorescein to induce thrombosis in cerebral microvessels. Thrombosis occurred only in the illuminated field, and only in the presence of both light and dye. Light/dye induced thrombosis does not depend on radiation or heat generation from the light when the light intensity (irradiance) is low. Hyperthermia due to light/dye treatment occurs when the irradiance exceeds 200 mW/cm^2 (Leunig *et al.*, 1994). The mechanism by which light/dye induces thrombosis may be due to the release of reactive oxygen species (ROS), especially singlet oxygen (Valenzeno, 1987), after the dye is excited

by the light. As for PDT, the effect of light/dye depends on light dose and dye concentration. **Table 1.1** shows typical cases of thrombosis induced by PDT and light/dye treatments under various light doses and dye concentrations.

Ultrastructural observations by electron microscopy found that light/dye induced microvascular thrombi consist primarily of platelets, rarely or no fibrin (Rosenblum *et al.*, 1977), and occasionally leukocytes in venules. No endothelial denudation was found (Rumbaut *et al.*, 2004).

Table 1. Pervious studies on PDT & light-dye treatment

Author	photo-sensitizer	dose	injection location	time applying before PDT	treatment location	wavelength (nm)	power (mW/cm^2)	treatment duration (min)	energy (J/cm^2)	Results, Notes
Chen et al., 2006	verteporfin	0.25/1.0 mg/kg	i.v. (rat)	15 min/3 hr	prostate tumor	diode laser, 690	50	16.7	50	vascular permeability increase, cell adhesion leading to thrombosis
Dolmans et al., 2002	MV6401	0.072, 0.036, 0.018 mg/kg	i.v. (mice)	15 min	mammary	diode laser, 664	50	1.7	5	acute temporal vasoconstriction (no thrombosis); long term vascular shutdown by thrombosis
Fingar et al., 1998	benzoporp-hyrin derivative monoacid ring A	2 mg/kg	tail vein (rat)	5 - 180 min	cremaster muscle	argon laser, 690	75	33.3	150	treatment 5/30 min after BPD inject. Completet occlusion of tumor microvessel, no in normal; 180min had no acute response in both
Kubler et al., 2003	mTHPC	0.3mg/kg	ear vein (rabbit)	24 - 96 hr	carotid artery, internal jugular vein	diode lasre, 652	100	1.7, 3.3	10,20	24 hr interval & 20 J causes severe edema, media-hyperplasia, endothelial layer loosen leading thrombosis.
Michels et al., 2003	verteporfin	6 mg/m^2	i.v. (human)	5 min	choroidal neo-vascularization	diode laser, 689	600	1.4	50	in human w. CNV not induce immediate thrombosis, primarily caused vascular barrier breakdown
Nagamine et al. 2002	Porfimer sodium	2, 1, 0.2 mg/kg	i.v. (rabbit)	5 min	auricular vein	argon, 630	300	5, 10, 15 each	90, 180, 270	In group 1, 2, sig. flow decrease after 15 min,sig. thromb grade 5/15 min
Sato et al. 1990	NaF	50 mg/kg	external jugular (rat)	simultaneously	mesentery	mercury lamp, 400-500	20.7 / 9.2 (mW/mm^2)	continuous	6.21	Thrombus induced in ti: 12±4 /52±28 s, total occlusion in ts: 139±35 / 457±201 s
Sato et al. 1984	NaF	50 mg/kg	external jugular (rat)	simultaneously	mesentery	mercury lamp, 400-500	2.4 (mW/mm^2)	continuous	7.21	Thrombus induced in ti: 418±109 s, total occlusion in ts: 3516±186 s

The endothelial glycocalyx layer and thrombosis

It has been known that the surface of endothelial cells forming the blood vessel wall is coated with a fluffy glycocalyx layer (**Fig. 1.2**, Squire *et al.*, 2001). The glycocalyx mainly consists of sulfated proteoglycans, hyaluronan, glycoproteins, and plasma proteins (Weinbaum *et al.*, 2007). The primary function of the glycocalyx layer is to serve as a barrier to macromolecule diffusion and blood cell adhesion to the endothelium and as a mechanotransducer of fluid shear stresses to the actin cortical cytoskeleton of the endothelial cell (Weinbaum *et al.*, 2007). Studies have suggested that this endothelial surface glycocalyx layer may also affect the hemodynamic parameters in the microcirculation including hematocrit and flow resistance (Pries *et al.*, 2000).

Degradation of glycosaminoglycans of glycocalyx increased capillary permeability and leukocyte adhesion, and diminished resistance to blood flow in the circulation (Adamson, 1990; Mulivor *et al.*, 2002; Pries *et al.*, 2000). Shedding of heparan sulfate from the glycocalyx resulted in increased endothelial cell sensitivity to activation by cytokines (Bode *et al.*, 2006). The disruption of the endothelial glycocalyx layer would result in adhesion of platelets and blood cells to the vessel wall as well as increase vascular leakages to macromolecules (Mulivor *et al.*, 2002; Reed *et al.*, 1988; Vink and Duling, 1996).

Previous studies demonstrated that light/dye treatment increased macromolecules penetration in the endothelial surface glycocalyx (ESG) of the

vascular wall, increased capillary tube hematocrit and the functional capillary diameter for erythrocytes in small capillaries of hamster cremaster muscle (Vink and Duling, 1996). Light/dye treatment was also reported to degrade the glycocalyx in mouse cremaster venules, reducing its thickness by 60-70% (Smith *et al.*, 2003; Damiano *et al.*, 2004).

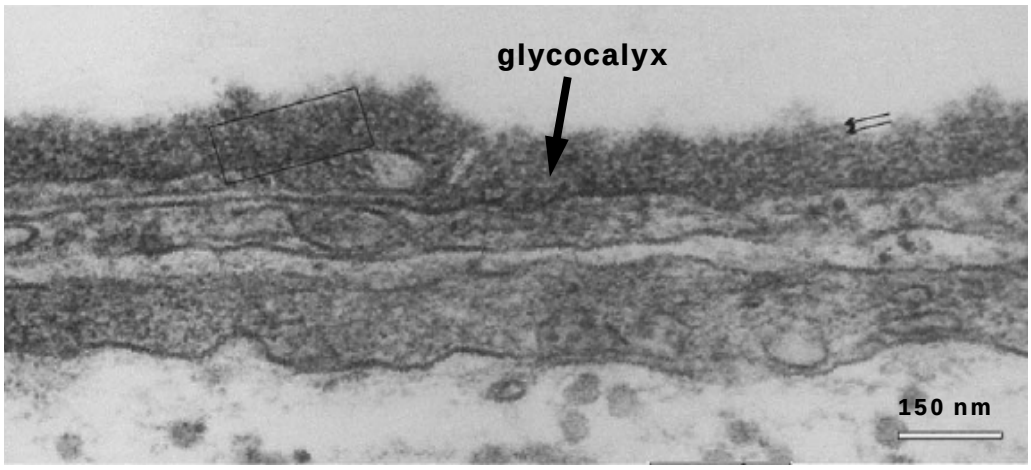

Fig. 1.2 Electron micrograph of endothelial glycocalyx at a microvessel wall (Squire *et al.*, 2001).

Objectives of the study

Previous studies have led to some understanding on the mechanical mechanism of the thrombus formation, but they were conducted under the conditions that the flow was either retarded or disturbed, or the vessels were injured/damaged by

using electrical, biochemical, light-dye treatment, or photochemical means. However, the quantitative understanding of their contribution to thrombosis was poor, especially in intact microvessels under laminar flow conditions. Therefore, the first objective of my thesis study was to investigate the relation between localized shear rates/stresses and thrombosis in intact bent microvessels with low Reynolds number blood flows.

To search for an effective method to prevent unwanted thrombosis from PDT or light/dye treatment, one needs to understand not only the chemical and molecular mechanisms by which light/dye induces thrombosis, but also the structural mechanisms by which light/dye ultimately affects the structural components of the microvessel wall. Therefore the second objective of this study was to test the hypothesis that light/dye induces microvessel hyperpermeability and thrombosis by destroying the integrity of the structural components of the microvessel wall, specifically, by degrading the endothelial surface glycocalyx.

CHAPTER 2 MECHANICAL MECHANISMS OF THROMBOSIS IN INTACT BENT MICROVESSELS OF RAT MESENTERY

Introduction

Thrombosis is the formation of blood clots in blood vessels. It is a direct cause for a stroke, a myocardial infarction and atherosclerosis. Although both biochemical and mechanical factors are found to play a role in thrombosis, the quantitative understanding of their contribution is poor, especially in the microvasculature with non-disturbed laminar flows. The objective of this study is to investigate the relationships between localized shear rates/stresses and thrombosis in bent microvessels with low Reynolds number blood flows

Previous studies found three possible causes for venous thrombosis (Hume *et al.*, 1970): (1) a primary lesion in the endothelium that produces an inflammatory reaction and then thrombosis occurs; (2) a slowed flow or other abnormality of flow resulting in the adhesion of formed elements to the intima which leads to thrombosis; (3) an increase of blood coagulability from changes in the physical and/or chemical properties of plasma. Venous thrombi may develop by one or the combination of these factors. For example, if there is a lesion, i.e. an opening of gaps between endothelial cells, invoked by local factors in the endothelium, platelets will adhere to these gaps where basement membrane is exposed and thrombus will form as a consequence.

Both mechanical and chemical factors can affect the activity of platelet coagulation factors responsible for the formation of thrombus near an injured/damaged vessel. O'Brien (1990) found that shear stress alone induced platelet aggregation in a manner similar to that observed on injured vessel walls. Muga *et al.* (1995) also demonstrated that hydrodynamic forces and geometric changes can induce thrombosis without the addition of chemical agonists by an experiment of blood flowing through a capillary tube in which a local hemostatic plug was formed following the production of a small hole on the tube wall. The attachment of platelets to the vessels wall and the rate of platelet aggregation increases (Turitto and Hall, 1998) when shear rate increases. The endothelial cells can become antithrombotic or prothrombotic depending on the magnitude and duration of the shear forces applied (Grabowski, 1995; Reinhart, 1994). In regions of irregular geometry, such as branches or stenoses, endothelial cells become prothrombotic, which may lead to platelet aggregation and fibrin formation (Holme *et al.*, 1997; Noren *et al.*, 2000). Studies (Sato and Ohshima, 1990) on microvessels (arterioles/venules) of rat mesentery indicated that thrombus initiation depended significantly on the shear rate rather than the flow velocity. In their experiments, the microvessels were pre-treated with irradiation method. It was observed that platelet thrombi were first initiated at the locations with higher shear rates in venules but at the locations with lower shear rates in arterioles.

While aforementioned studies have led to a better understanding of the mechanical mechanism for the thrombus formation, all these studies have been

conducted under the conditions that the flow is either retarded (flow stasis) (Nicolaides *et al.*, 1972; Wessler, 1962) or disturbed (secondary flow) (Chen and Lu, 2004; Wootton and Ku, 1999), or the vessels are injured/damaged by using electrical (Massad *et al.*, 1987; Wong *et al.*, 2000), biochemical (Begent and Born, 1970), light-dye treatment (Sato and Ohshima, 1990; Sasaki *et al.*, 2004; Seiffge and Kremer, 1986) or photochemical means (Rucker *et al.*, 2002). In this chapter, we developed a new experimental method to test the hypothesis that thrombi can be formed in bent/stretched microvessels with normal laminar blood flow by the localized hydrodynamic stimuli.

Materials and methods

Experimental methods

Experiments were performed on rat mesentery. All procedures have been approved by the Animal Care and Use Committees at the City College of the City University of New York. Female Sprague-Dawley rats (250–300 g) were supplied by Hilltop Laboratory Animals (Scottdale, PA). Rats were anesthetized with pentobarbital sodium given subcutaneously at the initial dosage 65 mg/kg and additional 3mg/dose as needed. After a rat was anesthetized, a midline surgical incision (2–3 cm) was made in the abdominal wall. The mesentery was gently taken out from the abdominal cavity and arranged on the surface of a polished quartz pillar (2cm in diameter, Heræus-Amersil, Fairfield, NJ) to maintain the circulation to the gut and mesentery of the animal. This also allowed the transillumination of the

mesenteric microvasculature. The upper surface of the mesentery was continuously superfused by a dripper with Ringer solution at 35–37 ^{o}C. A Nikon Eclipse TE-2000 inverted microscope with a 10× lens (NA 0.3, Nikon) was used to observe the mesentery. The microvessels chosen for study were straight, non-branched post-capillary venules (diameters 20–50 μm). All vessels had brisk blood flow and had no marginating white cells before they were bent and stretched. Mammalian Ringer solution was used for all dissections and superfusion (Fu and Shen, 2004; He *et al.*, 1998).

With the mesentery and a chosen microvessel under observation, a rounded-tip glass restraining micropipette (see arrow pointed object in **Fig. 2.1a**) was used to bend the microvessel at the nearby tissue. Cautions were taken during the manipulation to induce no/minimum damages to the vessels. We checked the possible minor damage by injecting fluorescence molecule, FITC-Dextran 70 K, into the circulation. This size molecule is hard to cross the intact microvessels. We did not see the fluorescence leakages during bending/stretch in five test experiments but we did see thrombosis in one of the vessels in ~30 min. The circulation in the microvessel was observed by a COHU CCD video camera and recorded in a video camera recorder. Off-line analysis was performed to obtain the flow velocity, size and bending angles of the vessels.

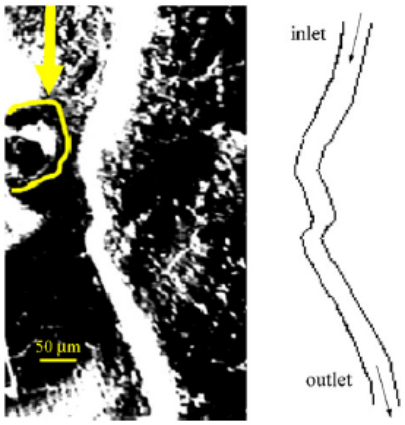

(a)

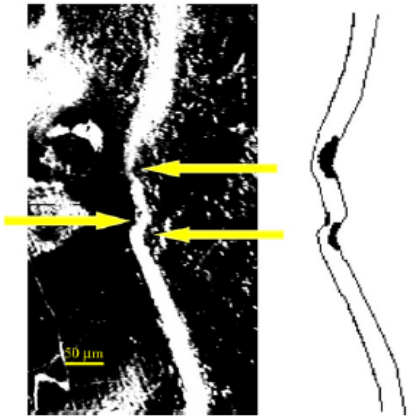

(b)

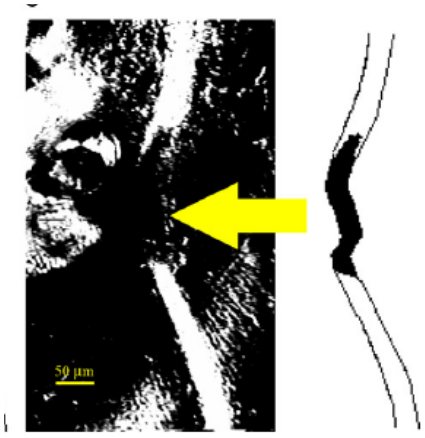

(c)

Fig. 2.1 Experimental observations for thrombosis in a bent post-capillary venule of rat mesentery in vivo. (a) The microvessel was bent/stretched by a restraining glass micropipette (pointed by the arrow) in the nearby tissue; (b) after the vessel was bent/stretched for ~ 3 min, blood cells accumulated at the inner side of three curved sites (indicated by the arrows); (c) in ~10 min after being bent/stretched, the vessel was completely blocked. Figures on the left are images taken in the experiment, and the ones on the right are the corresponding sketches.

Mathematical formation

Three-dimensional microvessel geometry was constructed using SolidWorks (SolidWorks Corporation, Concord, MA) as shown in **Fig. 2.2**. One microvessel with the similar curvature as that observed in the experiment was created (~90^o, **Fig. 2.2a**). The vessel has a circular cross-section with diameter 25 μm. For comparison, we also created microvessels with 0^o (straight) and 180^o curvature. For these three cases, the midline of the curved segments is of the same length *AB*. Prior to *A* and after *B*, the segments are straight and the entrance velocity conditions at *A* are the same for all three cases. The cross-section of the microvessel was taken to be circular as well as elliptic for the effect of deformation under stretch. We considered a representative elliptic cross-section with the radius of the longer axis twice that of the shorter axis in our model (**Fig. 2.2b**). The perimeter of the cross-section was assumed to be the same before and after deformation if the microvessel only changed its shape during the stretch.

This three-dimensional microvessel geometry was imported into Gambit, a CFD preprocessor, for volume meshes. A total number of 609,840 – 1,521,340 hexahedral elements were generated for various vessels. The computations were performed by using FLUENT 6.1.22 (Fluent Inc., Lebanon, NH). The flow in the microvessel had a mean velocity of 1mm/s (from our measurement) and was steady as it was far from the heart. The microvessel wall was taken as impermeable since the radial velocity across the vessel wall in a healthy vessel is about five orders of magnitude lower than the mean axial velocity. Blood was first approximated as an

incompressible and homogeneous Newtonian fluid with the density 1050 kg/m^3 and the effective viscosity μ = 2.5 cP in the microcirculation (Levenson *et al.*, 1990). We later compared the effect for non-Newtonian fluid. The Reynolds number of the flow in the microvessel was ~0.01. No-slip boundary condition was applied along the vessel wall. The continuity and Navier–Stokes equations were solved with a segregated solver in FLUENT.

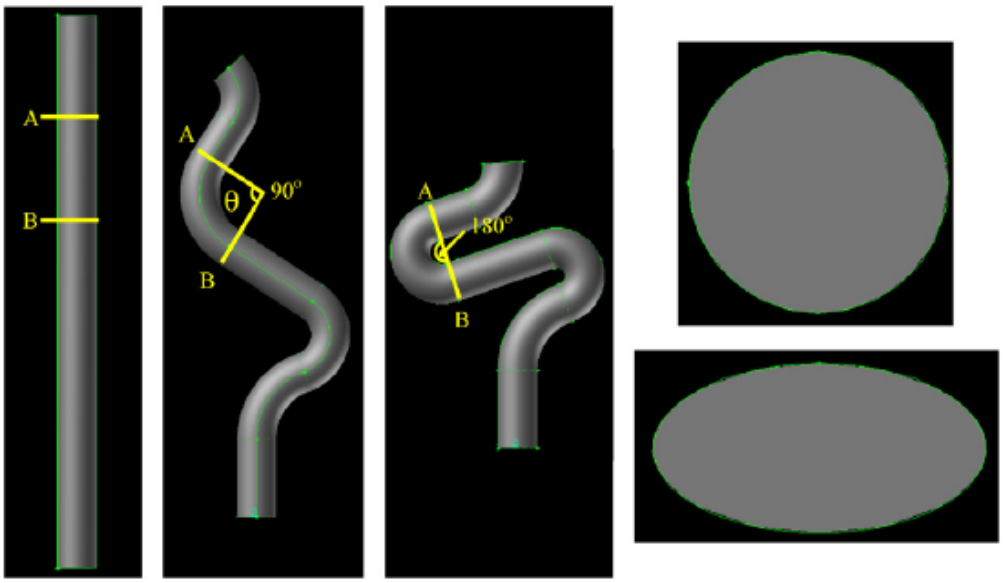

(a) **(b)**

Fig. 2.2 Model geometries: (a) vessels with three bending angles, straight (0^o), 90^o and 180^o. The segments are straight prior to the cross-section *A* at the upstream and after the cross-section *B* at the downstream. The entrance velocity conditions for the cross-section *A* and the midline length from *A* to *B* of section *AB* are the same for all three curved vessels; (b) vessels with circular and elliptic cross-sections due to deformation under the stretch. The circumference is the same for the circular and elliptic cross-sections.

Results

Experimental results

We observed that thrombi were initiated at the inner side of the curved vessels at 19 out of 61 curved sites (31.1%) in 48 bent/stretched vessels (**Fig. 2.3**) after the vessels were bent/stretch for 10 – 60 min. In a representative vessel shown in **Fig. 2.1**, the thrombi started to form in ~2 min after bending at three inner curved sites (**Fig. 2.1b**). In ~10 min, the vessel was completely blocked (**Fig. 2.1c**). **Figure 2.3** demonstrates that thrombosis more likely occurred at the curved inner site in the more bent vessels with diameters 25 – 30 μm (see Discussion later). In contrast, thrombosis was observed in none of 18 straight microvessels under the same experimental conditions.

The measured centerline red blood cell (RBC) velocities in the microvessels before and after bending were 1.57 ± 0.15 (SD) mm/s and 1.54 ± 0.14 (SD) mm/s (n = 16), respectively. There was no significant difference between these velocities ($p > 0.5$). The mean velocity of the bulk blood flow is about 1 mm/s, which is 1/1.6 of the centerline RBC velocity (Baker and Wayland, 1974). We use this mean velocity in our computational simulation. The mean velocity in the larger vessels (40 – 50 μm diameter) are slightly slower (~10% less) than that in the smaller vessels (20 – 30 μm diameter).

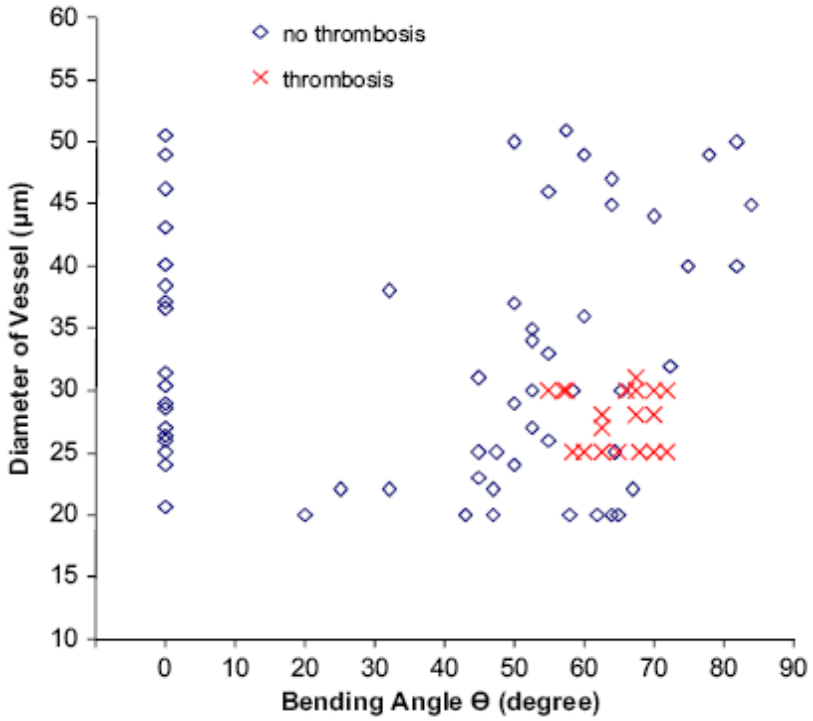

Fig. 2.3 Experimental data for the effect of the bending angle θ (**Fig. 2.2**) on thrombosis in various sized vessels. The crosses represent the bent vessels where thrombosis occurred while the diamonds represent the bent or straight vessels with no thrombosis.

Computational results

The velocity and shear rate distributions shown in the figures are plotted at the midplane of the vessel except otherwise specified. For the flow in the vessels with elliptic cross-sections, the plots are at the midplane with longer axis.

Figure 2.4 shows the velocity distributions in vessels with different curvatures and cross-sections. **Figure 2.4a–c** shows the results for the circular vessels

with bending angles 0^o (straight), 90^o and 180^o, respectively. **Figure 2.4d–f** is for the corresponding elliptical vessels. In addition to the distributions on the midplane, velocity contours at the cross-sections along the vessel are demonstrated on the right-hand side of each plot. In straight vessels (**Fig. 2.4a** and **d**), the flow is the Poiseuille flow in which the maximum velocity of 2 mm/s is at the centerline. When the vessels are bent to 90^o, the maximum velocity shifts from the centerline towards the inner side of the curve, and the value increases slightly (**Fig. 2.4b** and **e**). When the vessels are bent to 180^o, the maximum velocity shifts further towards the inner wall and increases to 2.02 and 2.13 mm/s respectively in circular and elliptic cross-sectioned vessels (**Fig. 2.4c** and **f**).

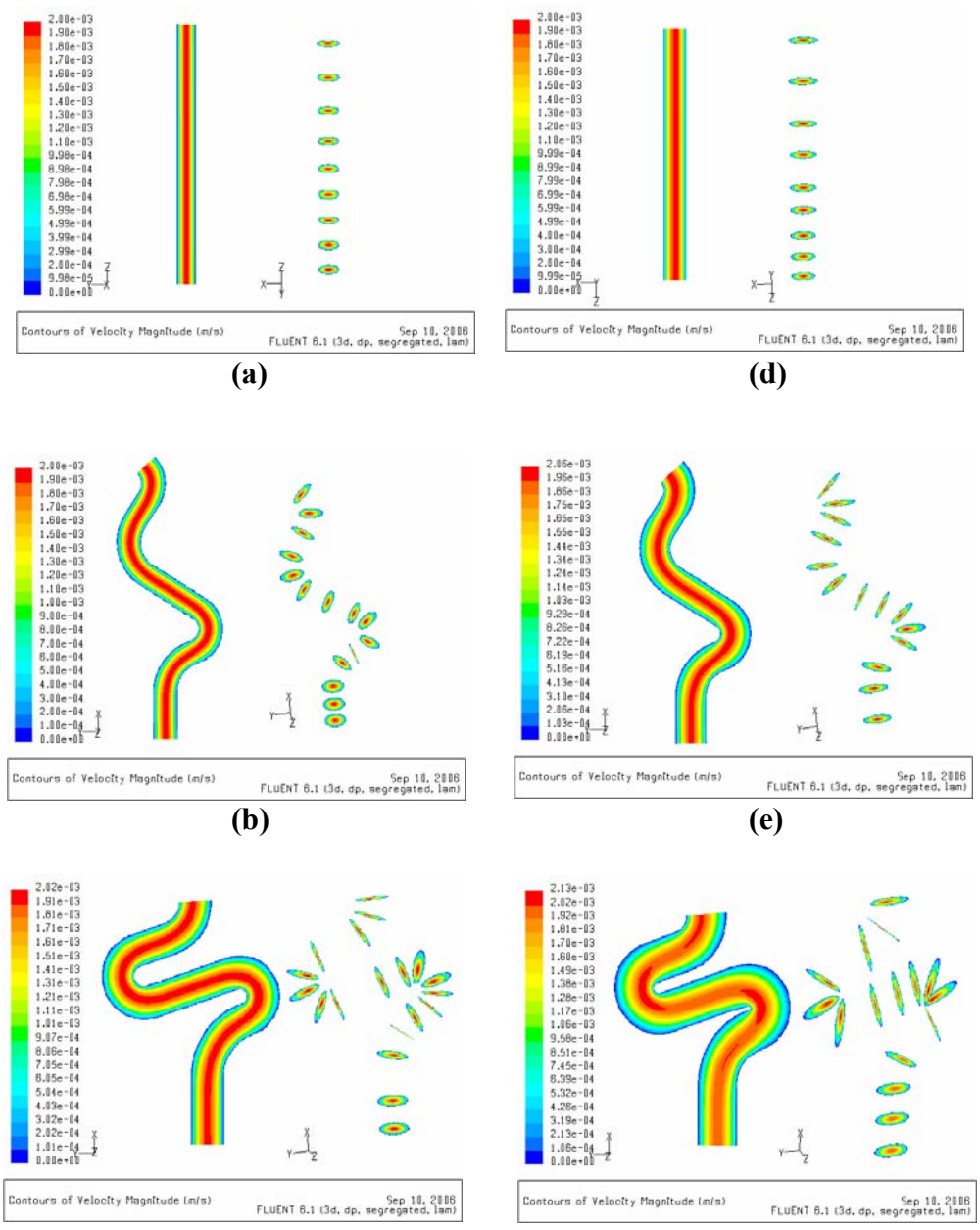

Fig. 2.4 Contour plots of velocity profiles in the midplane of the vessels. (a–c) are for vessels with circular cross-section; (d–f) are for vessels with elliptic cross-section. The figures on the right in each case are velocity profiles at the cross-sections along the vessel.

Figure 2.5 shows the corresponding shear rate distributions. For the flow in circular straight vessels, the shear rate is symmetrical about the axis, zero at the centerline and the maximum (320 l/s) at the wall (**Fig. 2.5a**). For the vessel with the elliptic cross-section, the maximum shear rate (493 l/s) occurs at two apexes on the wall with shorter axis radius (**Fig. 2.5d**). When the vessels are bent to 90^o, the zero-shear rate line shifts from the center towards the inner side of the curved vessel. The maximum shear rate increases from 320 to 509 l/s and occurs at the innermost wall of the curved vessel with the circular cross-section. While it increases from 493 to 606 l/s in the vessel with the elliptic cross-section at two locations close to the innermost side of the curve (**Fig. 2.5e**). **Figure 2.5c** and **f** shows the shear rate distributions in the vessels with 180^o curvature. The maximum shear rate further increases to 677 and 1000 l/s, respectively. The zero-shear rate line shifts even more towards the inner side of the curved vessel compared with that of 90^o curvature. In the elliptic vessel, the two locations with the maximum shear rate also shift closer to the inner side of the curved vessel.

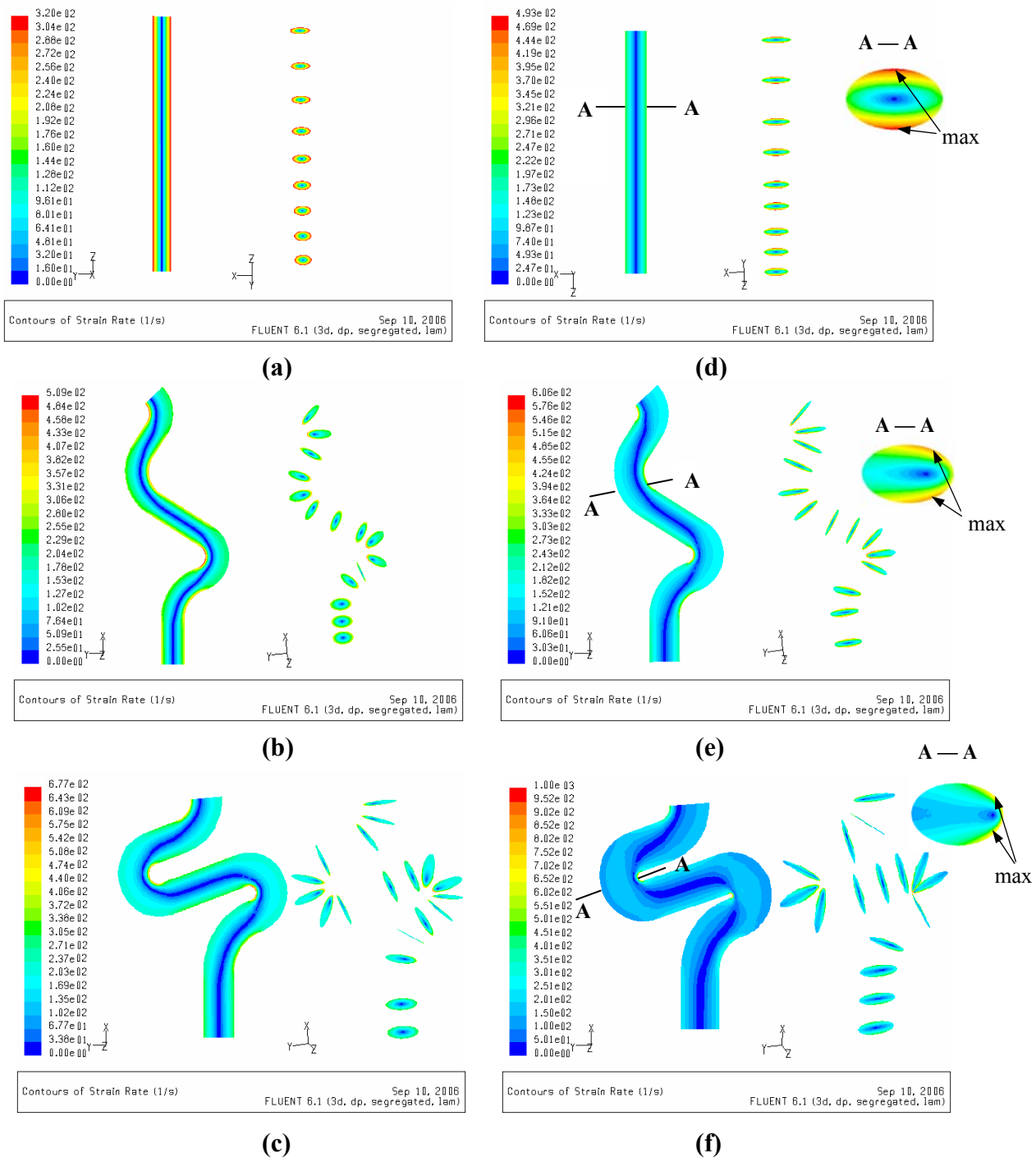

Fig. 2.5 Contour plots of shear rate profiles in the mid-plane of the vessels. (a–c) are for vessels with circular cross-section; (d–f) are for vessels with elliptic cross-section. The figures on the right in each case are profiles of shear rates at the cross-sections along the vessel.

Figure 2.6 shows the velocity profiles as a function of angular coordinate θ (**Fig. 2.2**) along the longitudinal axis. The origin of the coordinate is located at the apex of the bent portion of the vessel. **Figures 2.6a, b**, and **c** are circular vessels with bent angles 0^o (straight), 90^o, and 180^o respectively. **Figures 2.6d, e**, and **f** are for the corresponding elliptic vessels. Velocities are plotted for the middle-line (the solid line with the diamonds), the line 1/4 vessel diameter far from the inner (the dash-dot-dash line with the circles) and the line 1/4 vessel diameter far from the outer (the dashed line with the triangles) walls. For straight vessels, the maximum velocity is constant along the centerline and the velocities at 1/4 diameter inner and outer lines are overlapped. For the bent vessels, the centerline velocity decreases from the straight portion towards the bent portion, with the minimum at the most bent point. The larger the bending angle, the smaller the velocity at the most bent point. However, the velocity along the 1/4 diameter inner line increases from the straight part to the bent part, with the most increase in the transition region from the straight to the bent/stretched portions. Along about half of the bent/stretched portion, the velocity is almost constant. This constant is smaller than that along the centerline for the less bent vessels, but becomes closer to the centerline value as the bending angle becomes larger or the cross section becomes elliptic. It almost overlaps with the centerline velocity for the 180^o bent vessel with the circular cross section (**Fig. 2.6c**) and overpasses the centerline velocity for the elliptic shaped vessel (**Fig. 2.6f**). In contrast, the velocity at the 1/4 diameter outer line decreases from the straight to the bent portions. The decreasing rate is almost the same as the increasing rate for the velocity along the 1/4 diameter inner line at the transition region. The velocity at the 1/4

diameter outer line is also constant along about half of the bent/stretched portion. The difference between the two constant velocities for the inner and outer lines becomes bigger when the bending angle becomes larger, or the cross section deviates more from the circular shape.

In **Fig. 2.7**, we plot the shear rate profiles as a function of angular coordinate θ (**Fig. 2.2**) along the longitudinal axis. The origin of the coordinate is located at the apex of the bent portion of the vessel. In the straight vessels (**Fig. 2.7a** and **d**), the minimum shear rate (or shear) at each cross-section occurs at the centerline while the maximum occurs at the walls. For the elliptic-shaped vessel, the maximum shear rate is at the apex of the wall with shorter axis. The values of these shear rates are constant with changing y for the straight vessels. However, when the vessels are bent, the shear rates at the centerline, at the inner wall, as well as the maximum shear rate for the elliptic-shaped vessel, increase from the straight to the bent portions during the transition, reach a plateau for about half part of the bent segment, and then decrease at the same rate as for the increase. While the shear rate at the outer wall behaves in an opposite way. The larger the bending angle, the higher the increase/decrease rate, the larger the plateau rate at the inner wall, the larger the difference between the plateau rates at the inner and the outer walls, and the larger the maximum shear rate for the curved elliptic-shaped vessels.

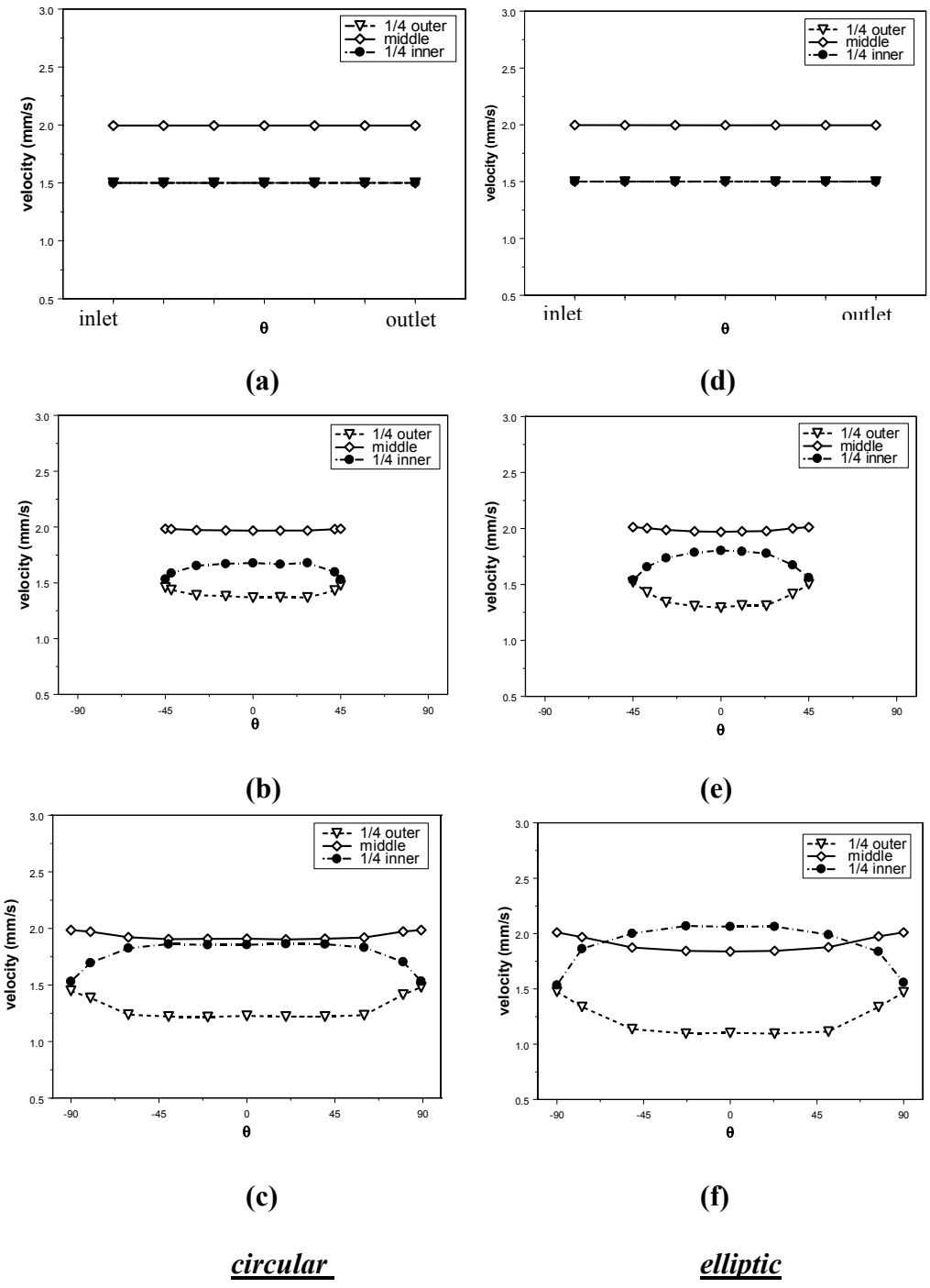

Fig. 2.6 Velocity profiles in the mid-plane along curved portion *AB* of the vessels. (a–c) are for vessels with circular cross-section; (d–f) are for vessels with elliptic cross-section. The solid line with the diamonds is for the velocity profile along the centerline, the dash-dot-dash line with circles and the dashed line with triangles are for those along the inner and the outer walls, respectively.

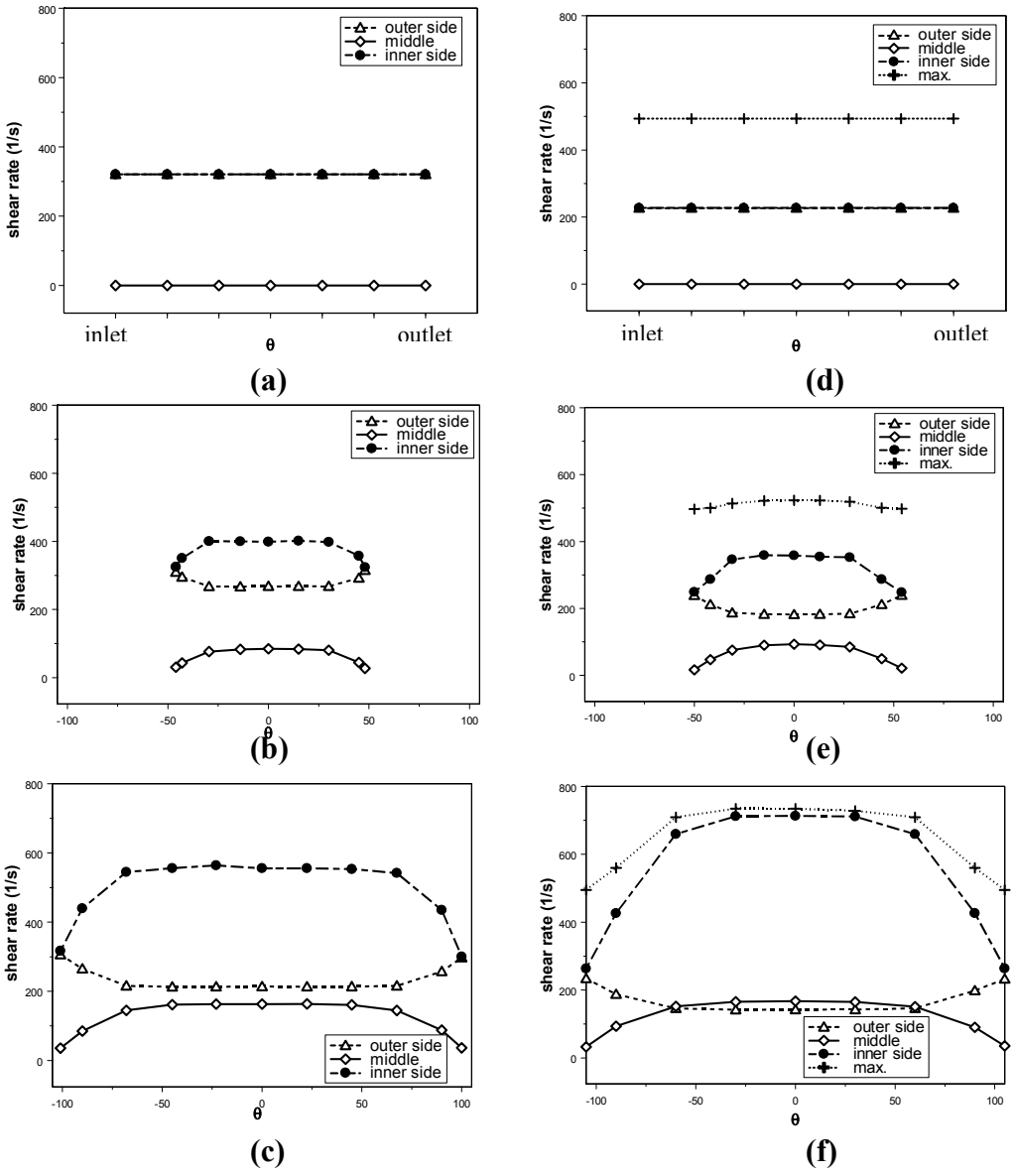

Fig. 2.7 Shear rate profiles in the mid-plane along the curved portion *AB* of the vessels. (a–c) are for vessels with circular cross-section; (d–f) are for vessels with elliptic cross-section. The maximum shear rate (see **Fig. 2.5**) is also plotted for the elliptic ones. The solid line with the diamonds is for the shear rate profile along the centerline, the dash-dot-dash line with circles and the dashed line with triangles are for those along the inner and the outer walls, respectively. The dotted line with crosses is the maximum shear rate at each cross-section for the elliptic shaped vessel.

Figure 2.8 shows the pressure distributions as a function of the distance from the point A for the bent/stretched portion A-B of the vessels (**Fig. 2.2**). The solid line with diamonds is for the pressure at the centerline, the dash-dot-dash line with circles for the pressure at the inner wall and the dashed line with triangles for that at the outer wall. These three lines are overlapped with each other indicating the pressure gradient in the radial direction is zero. The pressure differences over the bent/stretched segment A-B are 8.09 Pa, 8.15 Pa and 8.16 Pa for the straight, 90^o and 180^o bent/stretched circular vessels. They are 12.44 Pa, 12. 59 Pa and 12.70 Pa for the straight, 90^o and 180^o bent/stretched elliptic vessels.

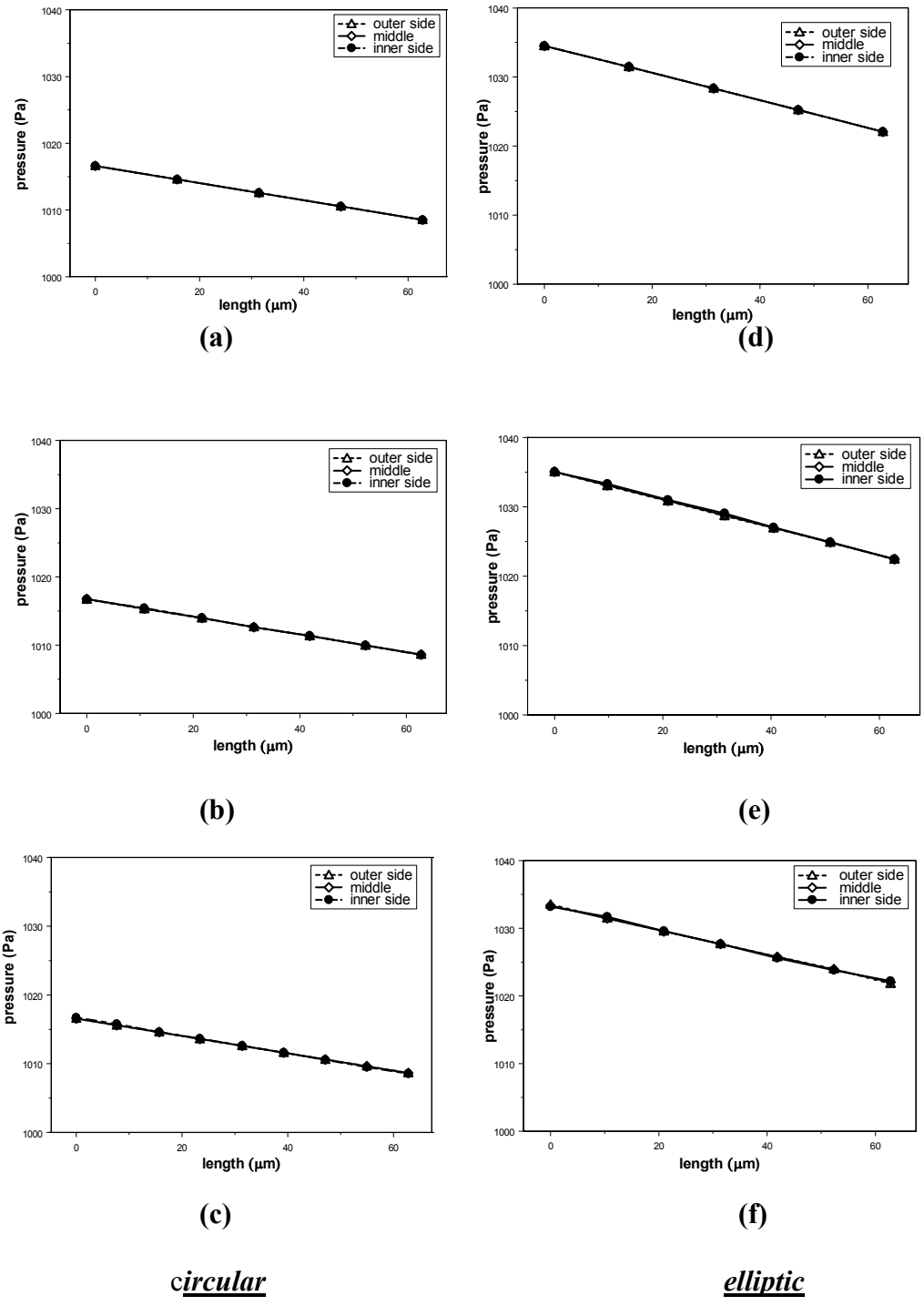

Fig. 2.8 Pressure profiles in the mid-plane along the curved portion *AB* of the vessels. (a) – (c) are for vessels with circular cross section; (d) – (f) are for vessels with elliptic cross section

Discussion

Effects of non-Newtonian fluid

It has been known that blood viscosity can be affected by hematocrit, plasma protein concentration and shear rate (Chien *et al.*, 1966). To evaluate the effect of non-Newtonian fluid, we used a Casson model for the blood (Das *et al.*, 1998, 2007). **Figure 2.9** compares the velocity and shear rate in the middle of section *AB* in circular vessels (**Fig. 2.2**) for Newtonian and non-Newtonian fluids. The maximum difference in velocities is < 6%, 4.5%, and 2.5%, for the straight, 90^{o} and 180^{o} curved vessels, respectively (**Fig. 2.9a**). Under very low shear rate, <50 s^{-1}, the difference in the shear rates for the Newtonian and non-Newtonian fluids can be up to 37%. However, most of the regions in our vessels have shear rates >100 s^{-1}, especially for the locations where thrombosis occurred (> 200 s^{-1}) (**Fig. 2.7**), thus the non-Newtonian effect is negligible under our study (**Fig. 2.9b**). Chien (1970) and Pries *et al.* (1992) also found that influence of the shear rate on viscosity appeared to be small in the microcirculation when shear rates were > 50 s^{-1}.

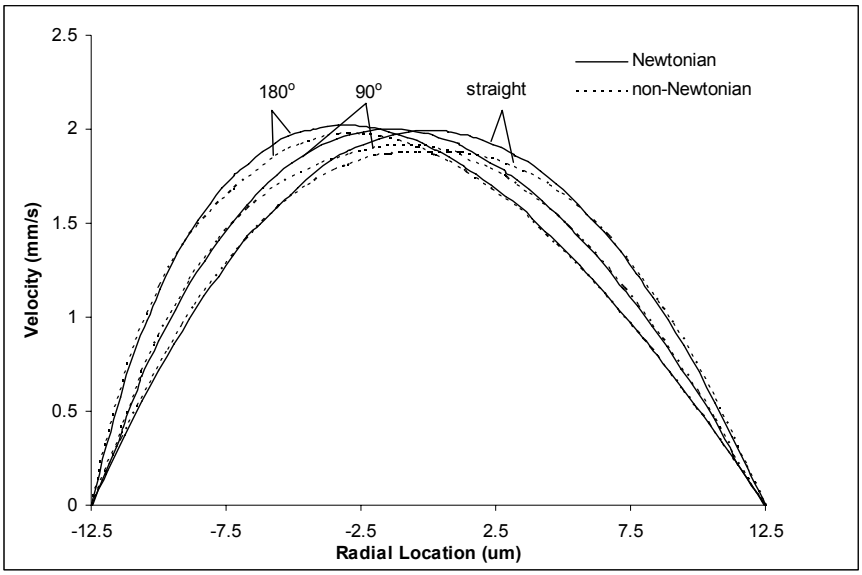

(a)

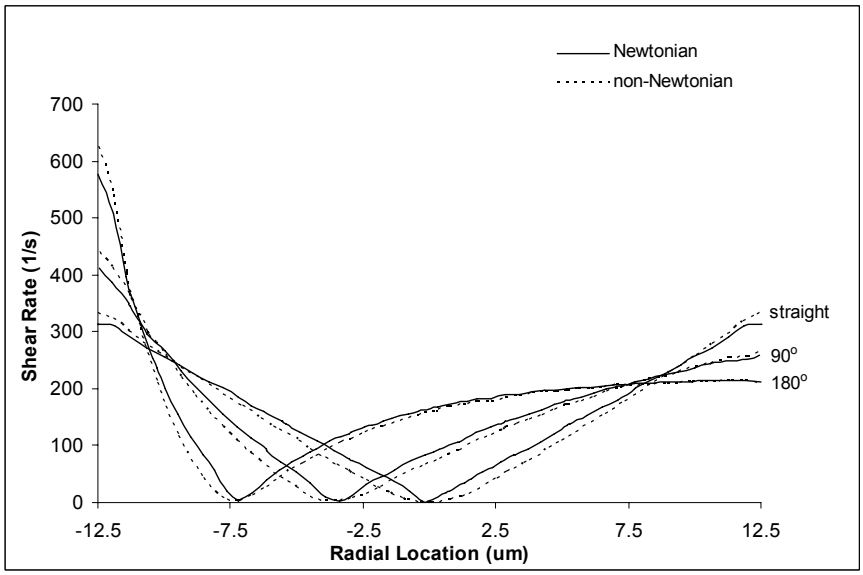

(b)

Fig. 2.9 Comparison of Newtonian and non-Newtonian fluid flow in circular cross-section microvessels: (a) mid-plane axial velocity profiles at the peak of the curved portion for Newtonian (solid line) and non-Newtonian (dashed line) fluid flow and; (b) mid-plane shear rate profiles at the peak of the curved portion for Newtonian (solid line) and non-Newtonian (dashed line) fluid flow. The non-Newtonian

viscosity μ_c is given by $\mu_c = [\mu_\infty^{1/2} + \tau_0^{1/2}/\gamma^{1/2}]^2$ where μ_c is the Casson viscosity, τ_0 is the yield stress and γ is the shear rate, $\mu_\infty^{1/2}$ and $\tau_0^{1/2}$ are given by Merrill *et al.* (1963), where α= 1.621, β = 0.627 (Das *et al.* 1998) and μ_p is the viscosity of Newtonian fluid, in our study μ_p = 2.5 cP in the microvessels (Levenson *et al.* 1990).

Effects of velocity on thrombosis

As shown in **Fig. 2.4**, although the centerline velocities were almost the same for the bent and straight microvessels, no thrombi were initiated in straight vessels. This suggests that thrombus formation is not correlated with the mean or centerline (maximum) blood flow velocities. Our results supported the conclusion in Sato and Ohshima (1990) study. However, for the bent vessels, the velocity near the inner wall is larger than that near the outer wall. The more the vessel is bent, or the more the vessel is stretched (from circular to elliptic), the bigger is the velocity difference. The larger velocity would carry more blood cells and more reactants to the inner vessel wall to increase the adhesion rate and accumulation of platelets to the wall (Turitto and Hall, 1998; Tangelder *et al.*, 1985).

Effects of stretch on thrombosis

Previous study found that converse compression of endothelial cells at the outer wall of the curvature may lead to cellular changes that retard the platelet thrombus formation, which is similar to vasodilation (Dai *et al.*, 2000). To test if the cellular morphology changes due to linear stretch (no curvature) induce thrombosis, we stretched the microvessels axially and transversely for ~60 min. In 10 axially

stretched microvessels, before the stretch, diameter = 29.2 ± 8.3 μm and centerline RBC velocity = 1.56 ± 0.21 mm/s (mean ± SD), and diameter = 28.1 ± 9.4 μm and centerline RBC velocity = 1.60 ± 0.21mm/s (mean ± SD) after the stretch (no significant changes, $p > 0.7$). Thrombosis was observed in none of the vessels. Neither did thrombosis occur in another four transversely stretched vessels. Our results indicate that stretch alone does not induce thrombi in post-capillary venules.

Effects of shear stress/rate on thrombosis

Because we approximated the blood as a Newtonian fluid, the shear rate is different from the shear stress only by a constant, blood viscosity. **Figure 2.5** and **2.7** demonstrate that the shear stress/rate at the inner wall is higher than that at the outer wall. The difference is bigger in more bent/stretched vessels. Our observation that the thrombus was initiated at the inner side suggests that the higher shear stress/rate causes thrombosis. **Figure 2.5** also demonstrates that the change in the shear stress/rate in the radial direction (the radial shear stress/rate gradient) is higher (the contour lines are denser) at the inner wall than that at the outer wall in the bent segment of the vessel. **Figure 2.5** and **2.7** show that the axial shear rate increases faster (the slope is steeper) at the inner wall from the straight to the bent segments, and it decreases faster from the bent to the straight segments. Both radial and axial shear stress/rate gradients at the inner wall become bigger when the vessels are bent more or distorted more from the circular shape, while those at the outer wall go the opposite way. These computational results reveal that the enhanced shear stress/rate

gradients at the inner wall in the curved vessels also affect thrombosis in the microcirculation.

The above predictions are consistent with our experimental results shown in **Fig. 2.3** except that we did not see thrombosis in smaller vessels (diameter ~20 μm) with the same bending angles (55 – 75^{o}) as in vessels of diameters 25 – 30 μm although the shear rate at the inner wall is 10 – 15% higher (**Fig. 2.10**). One explanation is that in this range of smaller vessels, the viscosity is smaller than that in larger vessels due to plasma skimming (Fahraeus–Lindqvist effect) (Lipowsky *et al.*, 1980). Higher viscosity will induce higher shear stress at the same shear rate. This suggests that shear stress is more important than shear rate in thrombosis in the microcirculation. Another observation from **Fig. 2.3** is that there was no thrombosis in larger vessels (diameter 40 – 50 μm) with somewhat larger bending angles (75 – 90^{o}). This is due to lower shear stress/rate in the larger vessels. **Figure 2.10** shows that at the same bending angle 90^{o}, the inner curved wall of 25 μm diameter vessel would experience the shear stress/rate that is ~1.5 times of that in 50 μm diameter vessel. For the straight ones, the difference in the wall shear stress/rate would be two times for the same mean bulk flow velocity.

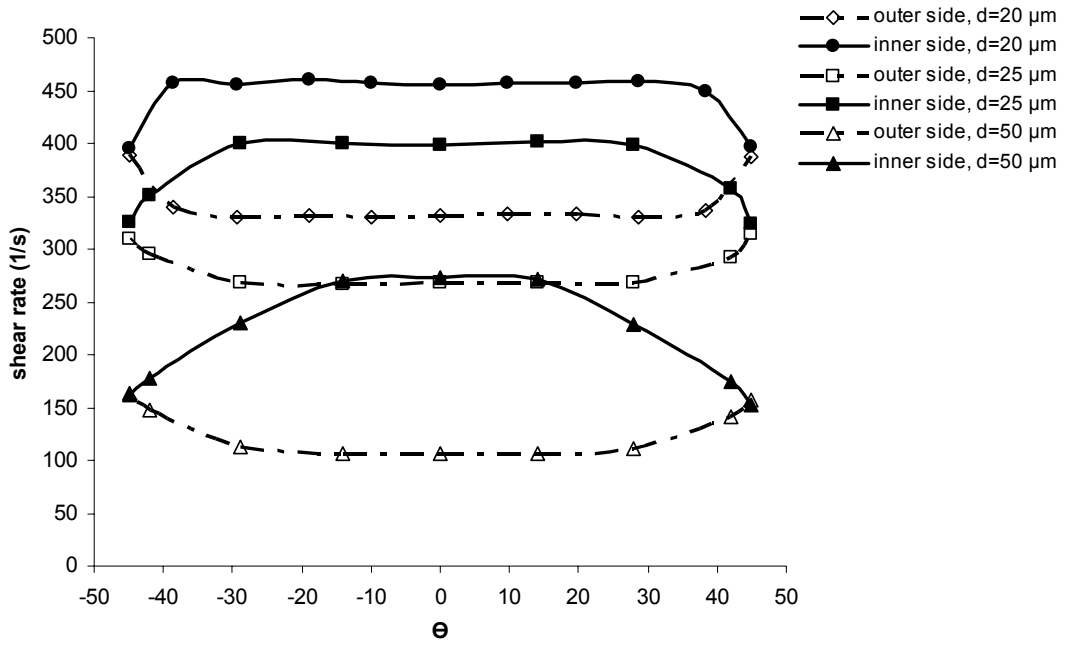

Fig. 2.10 Comparison of wall shear rates for different sized microvessels with the same bending angle $\theta = 90^{o}$.

The geometric change of the microvessel in our study, from a straight to a bent one, alters the magnitudes and distributions of the local hydrodynamic factors. The localized higher shear stress/rate and shear stress/rate gradient at the inner wall of the bent vessel activate the endothelial cells and the platelets, increase platelet adhesion to the endothelial cells and increase platelet aggregation and fibrin formation, and eventually, thrombus formation. Our results help to explain the development of micro-thrombi in bent/stretched microvessels, e.g., during long distance air travel or stay in a restricted space for a long period of time. When the micro-thrombi are brought by the blood flow to a major vein, deep vein thrombi would form and may induce death if they completely occlude the major pulmonary

circulation (Grabowski, 1995; Hume *et al.*, 1970). Another case is that deep venous thrombosis and pulmonary embolus happened in 1 of 200 cases after face-lift plastic surgery (Reinisch *et al.*, 2001; Most *et al.*, 2005). This may be also due to the bending and stretching in the microvessels during the operation.

CHAPTER 3 STRUCTURAL MECHANISMS OF LIGHT/DYE INDUCED MICRO-VASCULAR HYPERPERMEABILITY AND THROMBOSIS

Introduction

Photodynamic therapy (PDT), or light/dye treatment, has been widely used to treat a variety of cancers, including lung, skin, gastrointestinal tract, brain, head and neck, bladder, and pancreatic caners (Dolmans *et al.*, 2003). It is also used to treat age-related macular degeneration, cardiovascular diseases, actinic keratosis, and rheumatic diseases (Detty *et al.*, 2004; Dougherty, 2002; Dougherty *et al.*, 1998). The light/dye-mediated tumor destruction includes direct tumor cell killing, immune reaction, and vascular damage (Ortner and Dorta, 2006). Effects of PDT on tumor vasculature are vasoconstriction, thrombus formation, and vascular solute permeability increase (Chen *et al.*, 2006; Dolmans *et al.*, 2002; Fingar *et al.*, 1999; Nagamine *et al.*, 2002; Proske *et al.*, 2000).

PDT was shown to have the similar effects on normal blood vessels as well (Reed *et al.,* 1989). Light/dye induced thrombi were also observed in normal microvessels of rat mesentery (Sato and Ohshima 1984) and mouse cremaster muscle (Rumbaut *et al.,* 2004). Light/dye was found to decrease expression of thrombomodulin and increase expression of tissue factor, thus leading to an increased thrombogenic environment (Fungaloi *et al.,* 2003). Electron microscopic observation

of light/dye induced thrombi revealed that thrombi consist primarily of platelets and occasionally of leukocytes in post-capillary venules (Rumbaut *et al.,* 2004). The mechanisms for light/dye induced microvascular thrombosis include oxidative stress (reactive oxygen species generated upon excitation of the fluorochrome) and endothelial injury induced expression, activation of adhesion molecules on platelets, endothelial cells and leukocytes, and the accompanying recruitment of platelets and leukocytes to the vessel wall (Valenzeno and Pooler 1982; Sato and Ohshima 1990; Gaugler *et al.*, 1997; Hallahan and Virudachalam 1999; Thorlacius *et al.*, 2000; Mouthon *et al.*, 2003; Rumbaut *et al.*, 2004, 2005; Tailor *et al.*, 2005). Ultrastructural studies demonstrated that during minor and moderate light/dye treatment (less than 10 mW/mm^2), platelet adhesion and aggregation occurred in the absence of endothelial denudation or injury (Povlishock *et al.,* 1983; Rumbaut *et al.,* 2004).

Although large effort has been made to elucidate the molecular mechanisms by which PDT or light/dye induced thrombosis, our understanding for the structural mechanisms, or the ultimate effect of light/dye on the structural components of the microvessel wall, is poor. The cleft between the adjacent endothelial cells (inter-endothelial cleft) is the principal pathway for water and hydrophilic solutes transport across the microvessel wall under normal physiological conditions (Curry 1984; Fu *et al.,* 1994; Michel and Curry 1999). It is also suggested to be the pathway for transport of large proteins, platelets and leukocytes across microvessel walls in disease. **Fig. 3.1** shows a 3-D model for the inter-endothelial cleft (revised from Fu *et al.,* 1994). There are junction strands with discontinuous breaks within the cleft (Adamson *et al.*,

2004) and a surface glycocalyx layer (Squire *et al.,* 2001; Vink and Duling, 1996; Smith *et al.*, 2003; Damiano *et al.*, 2004) at the luminal entrance of the cleft. Light/dye treatment has been shown to increase the penetration of macromolecules in the endothelial surface glycocalyx layer, increase capillary tube hematocrit and the functional capillary diameter for erythrocytes in small capillaries (~5 μm diameter) of hamster cremaster muscle (Vink and Duling 1996). Using a microparticle image velocimetry, light/dye treatment was reported to degrade the glycocalyx in mouse cremaster venules (20-45 μm diameter), reducing its thickness by 60-70% (Smith *et al.*, 2003; Damiano *et al.*, 2004). Previous studies also suggested that this glycocalyx layer affects the vascular permeability, leukocyte-endothelial adhesion, and repair of the vessel wall (Fu *et al.,* 1994; Reed and Miller 1988; Fu and Shen 2003; Pries *et al.,* 2000; Mulivor and Lipowsky 2002).

As reported in previous studies, the degree of endothelial damages by light/dye treatments depends on the irradiation power of the light/dye and the length of treatments. The objective of our study was to investigate the common structural mechanisms by which the light-dye induces hyperpermeability and thrombosis in the microvessels of rat mesenteries *in vivo*. We hypothesized that light/dye destroys the integrity of the structural components of the inter-endothelial cleft to increase microvessel permeability and induce thrombosis. To test this hypothesis, we first quantified the microvascular thrombosis in terms of initiation time, growth rate, and the time for the complete microvessel occlusion. Then, we measured the microvessel hydraulic conductivity *Lp* and solute permeability P to TRITC-albumin (Stokes radius

~3.5 nm) under the similar light/dye treatment as for the thrombosis. Thirdly, we applied a mathematical model for the inter-endothelial cleft (revised from Fu *et al.*, 1994) to predict the possible changes in *Lp* and *P* to albumin by changing the structural components of the microvessel wall, e.g., degrading the surface glycocalyx, increasing the gap between endothelial cells, and increasing the size or the number of junction pores. Finally, we compared the measured *Lp* and *P* to albumin with those predicted and found the most likely structural changes induced by the light/dye treatment. Understanding the structural mechanisms of light/dye effects on the microvessel permeability and thrombosis is important for preventing unwanted side effects of PDT treatment on normal vessels.

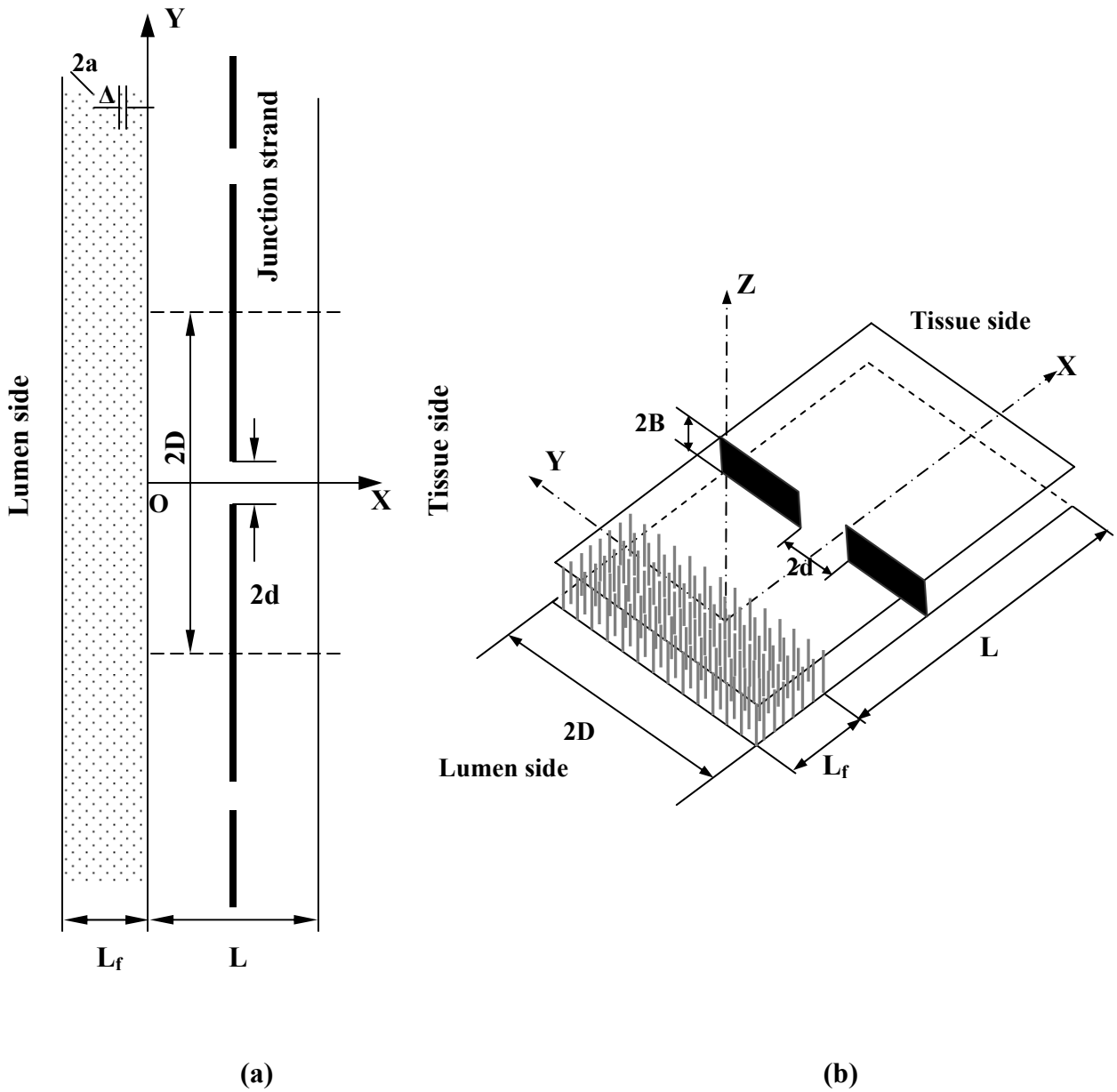

(a) **(b)**

Fig. 3.1 (a) Plane view of the model geometry for the interendothelial cleft in the wall of a rat mesenteric microvessel (revised from Fu *et al.*, 1994). A junction strand with periodic breaks lies parallel to the luminal front of the cleft. An endothelial surface glycocalyx layer (fiber matrix) of thickness L_f is at the cleft entrance; *2a* is the fiber diameter and Δ is the spacing between fibers; *L*, the total depth of the cleft; *2D*, the distance between two adjacent breaks in the junction strand; *2d*, the width of the junctional break. **(b)** Three-dimensional view. 2B, the width of the cleft.

Materials and methods

Animal preparation

Experiments were performed on post-capillary venules in rat mesenteries. All procedures and the animals used have been approved by the Animal Care and Use Committees at the City College of the City University of New York. Female adult Sprague-Dawley rats (age 3-4 months, 250-300 g) were supplied by the Hilltop Laboratory Animals (Scottdale, PA). Rats were anesthetized with pentobarbital sodium given subcutaneously at the initial dosage 65 mg/kg and additional 3 mg/dose as needed. After a rat was anesthetized, a midline surgical incision (2-3 cm) was made in the abdominal wall. The rat was then transferred to a tray and kept warm on a heating pad (Fu and Shen, 2004). The mesentery was gently taken out from the abdominal cavity and arranged on the surface of a polished quartz pillar (2 cm in diameter, Heræus-Amersil, Fairfield, NJ) to maintain the circulation to the gut and mesentery of the animal. This also allowed the transillumination of the mesenteric microvasculature. The upper surface of the mesentery was continuously superfused by a dripper with Ringer solution at 35-37^{o}C. The flow of superfusate was maintained at 3.5-4.0 ml/min to keep the layer of fluid over the tissue at an approximately constant depth. The microvessels chosen for study were straight non-branched post-capillary venules (diameters 30-50 μm).

Solutions and fluorescent test solute preparation

Mammalian Ringer solution

Mammalian Ringer solution was used for all the dissection and superfusion. The solution was composed of (in mM) 132 NaCl, 4.6 KCl, 1.2 $MgSO_4$, 2.0 $CaCl_2$, 5.0 $NaHCO_3$, 5.5 glucose, and 20 HEPES. The pH value was balanced to 7.4 - 7.45 by adjusting the ratio of HEPES acid to base (Fu and Shen, 2004; He *et al.*, 1998). The perfusate also contained 10 mg/ml BSA (bovine serum albumin, A4378, Sigma-Aldrich, St. Louis, MO), named as 1% BSA Ringer.

Sodium fluorescein

Sodium fluorescein (NaF, F6377, Sigma-Aldrich, St. Louis, MO) was used as the dye for the light/dye (NaF) treatment. NaF was dissolved in 1% BSA Ringer solution. The concentration of NaF for the systemic administration was 10 mg/ml, at the dose of 50mg/kg body weight, while the concentration of NaF for the single vessel perfusion was 0.5 mg/ml, which was calculated under the estimation that the total blood volume of a rat is ~ 20 ml (Probst *et al.*, 2006).

TRITC-BSA

Tetramethylrhodamine isothiocyanate-bovine serum albumin (TRITC-BSA, MW 67,000, Stokes radius ~3.5 nm, A2289, Sigma-Aldrich, St. Louis, MO) was used for solute permeability measurement. The TRITC-BSA was dissolved at 0.75mg/ml

in 1% BSA Ringer solution. All the solutions were made fresh on the day of use to avoid binding to the serum albumin.

Intravital microscopy

A Nikon Eclipse TE2000-E inverted fluorescent microscope was used to observe the mesentery. A 10× lens (NA 0.3, Nikon) gave a field of view of approximately 2 mm in diameter. The tissue was observed with either transmitted white light from a light pipe suspended above the preparation or with fluorescent light from an illumination system (the monochromator with a xenon lamp FSM150Xe, Bentham Instrument Ltd., UK). The monochromator can generate the light of wavelength from 200-700nm. The fluorescent (irradiation) light intensity was measured by a power meter (model 1815-C, Newport Corp., Irvine, CA). The process of thrombosis was monitored by a CCD video camera (CV-M50, JAI Corp., Japan) and recorded on a VCR. **Figure 3.2** shows the experimental setup.

Thrombosis induced by light/dye treatment

With the mesentery and a chosen microvessel under observation, the fluorescent light of 490 nm wavelength was turned on while sodium fluorescein (NaF) was simultaneously injected into the rat body through the carotid artery. The dosage of one dose injection with 10 mg/ml NaF was 50 mg/kg body weight. Thrombus growth was then observed and recorded. The experiment lasted until the microvessel was completely occluded by the thrombi. Then the fluorescent light was

turned off, another 30 min observation under the bright field was continued to see if thrombi could be washed away by the blood flow.

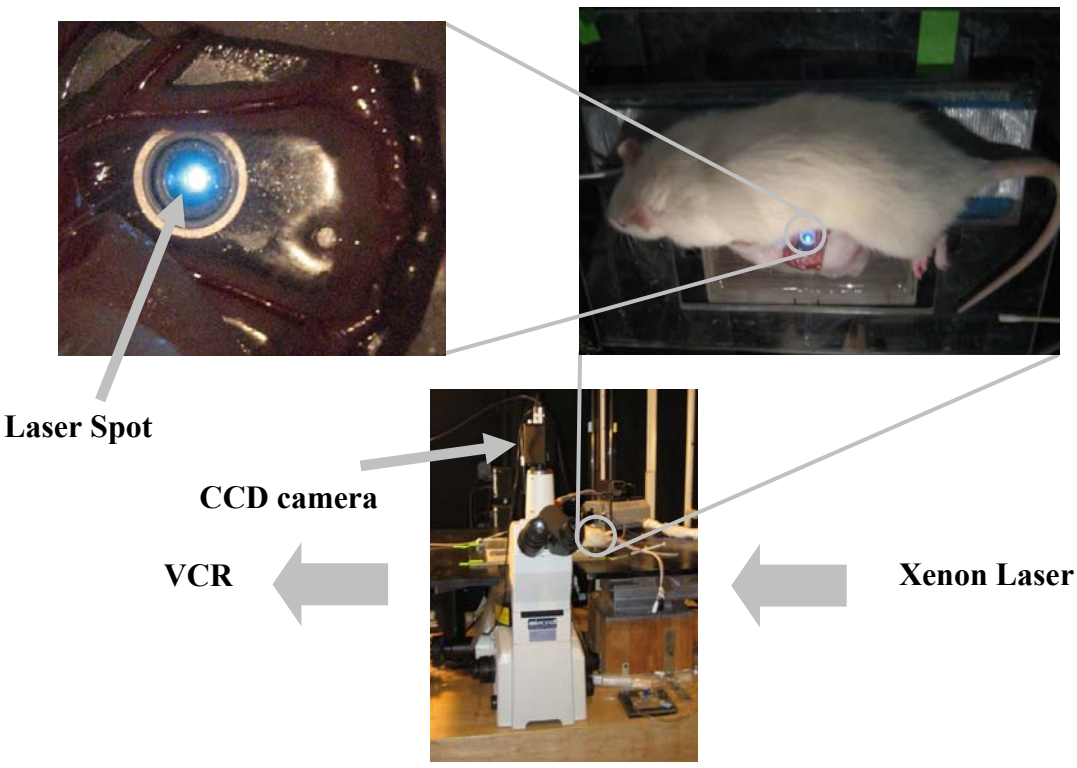

Fig. 3.2 Experiment setup. Laser was delivered through optical fiber to the microscope, and spread across the mesentery on the cover slip. The time course of the experiment was monitored by a CCD camera and recorded on a VCR.

Measurement of microvascular hydraulic conductivity Lp

Hydraulic conductivity *Lp* was determined using the modified Landis technique (Curry, 1984), which measured the volume flux of water across the microvessel wall (**Fig. 3.3**). A micropipette with the tip diameter of 10-15 μm, filled

with the marker cells (RBCs) in either a control solution of 1%BSA Ringer or the solution additionally containing 0.5 mg/ml NaF, was used to cannulate a single microvessel on a rat mesentery. The method for *Lp* measurement was briefly described in the figure caption for **Fig. 3.3**. To ensure that any changes in *Lp* after cannulation and perfusion were not caused by the recannulation procedure alone, in a matched sham control group, we measured the baseline *Lp* of a vessel perfused with 1% BSA Ringer, and then recannulated the same vessel and measured *Lp* in the same control solution for ~50 min. During the replacement of the pipette, the pressure was dropped to < 1 cm H_2O, so flow at the tip during recannulation could be neglected. The pressure was then set back to 30 – 60 cm H_2O for perfusion.

To test the effect of light/NaF on *Lp*, we first measured the baseline *Lp* of a vessel by perfusing 1%BSA Ringer; then recannulated the same vessel with a pipette additionally containing 0.5 mg/ml NaF when the vessel was simultaneously exposed to 0.37 mW/mm^2 fluorescent light of 490 nm wavelength. The *Lp* was measured after 2-5 min exposure to the light, (similar timing for thrombus initiation), then it was measured every 5 min up to 30 min. Finally we measured the *Lp* for another 20 min in the presence of 0.5 mg/ml NaF when the fluorescent light was turned off. To examine *Lp* change prior to onset of thrombosis, in another group of microvessels, we measured *Lp* every min from the beginning of the light/NaF treatment up to 10 min.

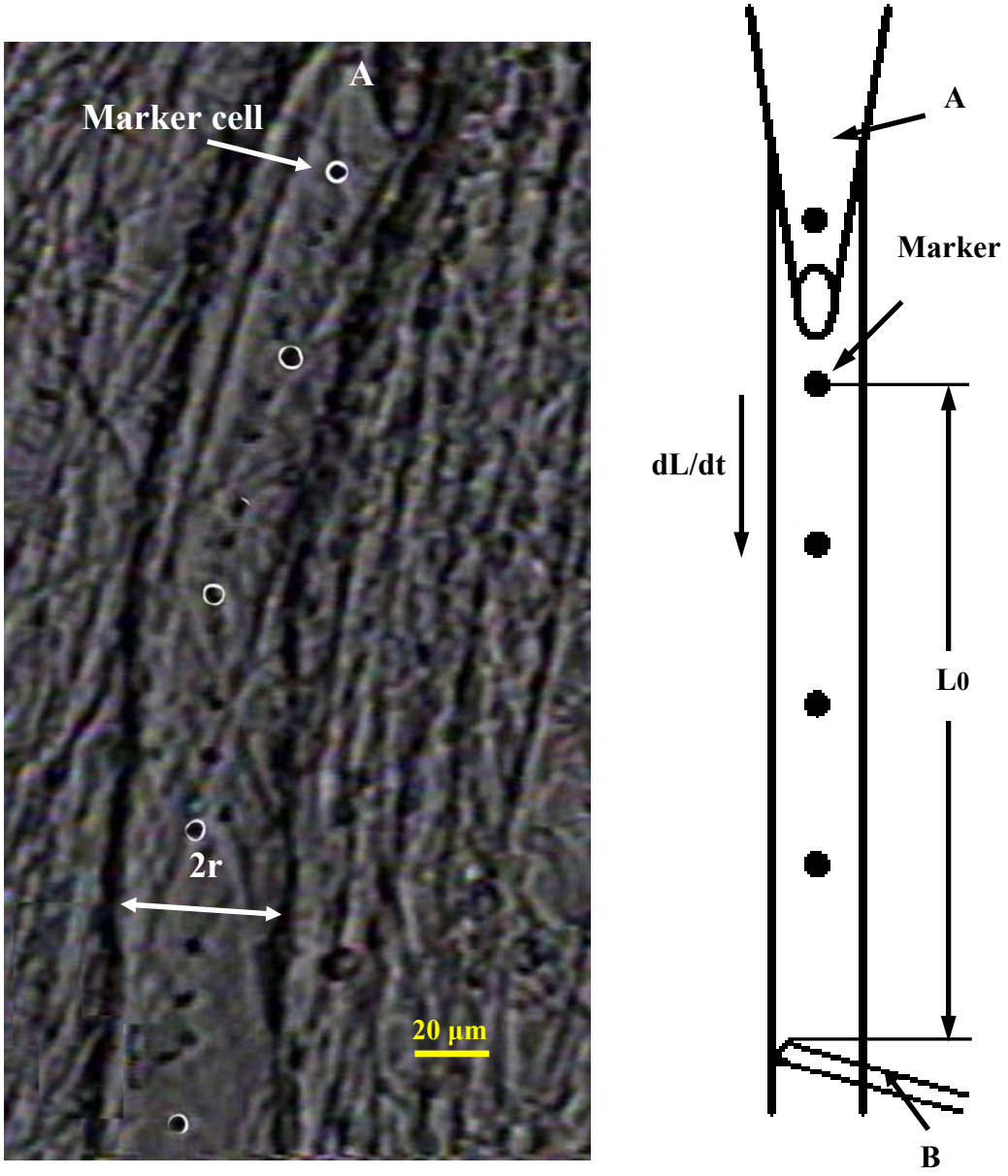

Fig. 3.3 Landis technique used to measure hydraulic conductivity *Lp*. Left panel shows a video image of a single microvessel of diameter *2r*, cannulated by a micropipette *A* (at the top) containing marker cells (red blood cells). The marker cells were perfused from the micropipette into the microvessel lumen at a known driving pressure created by a water manometer connected to the pipette *A*. If the downstream of the microvessel was blocked by an occluding micropipette *B*, *Lp* was calculated by $Lp = r/2 \times 1/L_0 \times (dL/dt)/\Delta p$, where Δp is the effective pressure difference across the

microvessel wall, *dL/dt* is the moving velocity of a maker cell when the vessel downstream was occluded, and L_0 is the distance between the marker cell at the entrance of the vessel and the occluding pipette *B* (right panel).

To compare the effect of light/NaF treatment with that of fluorescent light alone or NaF alone on the *Lp*, after baseline *Lp* measurement with 1% BSA Ringer, the same vessel was recannulated with the micropipette with the same 1% BSA Ringer (or additionally containing 0.5 mg/ml NaF), the *Lp* was measured after 2-5 min exposure to the fluorescent light (or without light exposure in the presence of NaF), then it was measured every 5 min up to 30 min. Finally the *Lp* was measured for another 20 min when the fluorescent light was turned off.

Although NaF concentration, 0.5mg/ml, in a perfused microvessel for the light/NaF effect on *Lp*, was similar to the local concentration in a microvessel during thrombosis (~10mg NaF in ~20ml blood of a rat), and the same irradiation power, 0.37 mW/mm^2, was applied in both cases, the thrombosis, however, occurred in the presence of blood cells. Due to the limitation of our technique for *Lp* measurement, we could only measure *Lp* in the absence of blood cells. To include the light/dye influence from the activated blood cells on *Lp*, we measured *Lp* at the initiation of thrombosis and when the vessel was 50-75% occluded by the thrombus. When the vessel was completely occluded, the perfusate with the marker cells failed to wash way the blockage and no *Lp* measurement was able to be taken. Therefore, *Lp* was measured when the vessel was partially occluded. Briefly, 10mg/ml NaF at 50mg/kg was injected through the carotid artery and circulated to a mesenteric microvessel

exposing to 0.37 mW/mm^2 light. At the initiation of thrombosis, a micropipette containing 0.5mg/ml NaF in 1% BSA Ringer and the maker cells was used to cannulate the microvessel, *Lp* was measured immediately and then every 5 min after exposure to the light for 30 min. Similarly, when a vessel was 50-75% occluded, a micropipette containing 0.5mg/ml NaF in 1% BSA Ringer and the maker cells was used to cannulate the vessel, *Lp* was measured immediately and then every 5 min after exposure to the light for 10 min.

Measurement of microvascular solute permeability P

To investigate the structural mechanism of thrombosis and *Lp* increase induced by the light/dye treatment, we also measured the microvascular solute permeability *P* to TRITC-BSA. Measurement of *P* was made on the individual post-capillary venules (40 – 50 μm in diameter). The detailed method using θ pipette was previously described in Fu and Shen (2004). Briefly, when TRITC-BSA was perfused into the vessel and the vessel was exposed to a 540 nm light at a much lower power of ~0.04 mW/mm^2, the images were recorded simultaneously. Then the *P* was determined off-line. The total fluorescence intensity (*I*) in the lumen of a straight vessel and surrounding tissue (**Fig. 3.4**) was determined by image analysis software (Intracellular Imaging Inc., Cincinnati, OH). The measuring window was 300 – 500 μm long and 100 – 200 μm wide and was set at least 100 μm from the cannulation site and from the base of the bifurcation to avoid solute contamination from the cannulation site and from the side arms. Permeability *P* was calculated by $P = (1/\Delta I_0)(dI/dt)_0(r/2)$ (**Fig. 3.5**)., where ΔI_0 was the step increase in fluorescence

intensity in the measuring window when the perfused dye just filled up the vessel lumen, $(dI/dt)_0$ was the initial rate of increase in fluorescence intensity after the dye filled the lumen and began to accumulate in the tissue, and r was the vessel radius. The assumption for using the above equation for determining the P was that the fluorescence intensity is linearly related to the fluorescence concentration. We did *in vitro* calibration experiments to test this assumption as described in Yuan *et al.* (2009). We used the same instrument settings in the calibration experiments as those used in the P measurement. The linear range of TRITC-BSA concentrations was from 0 to 1.25 mg/ml under our settings. We thus chose 0.75 mg/ml TRITC-BSA in our experiments.

To test P change under the light/NaF treatment, we used a θ pipette with two lumens separated by a septum (the cross-section looks like the Greek letter θ). We first measured the baseline P of a single vessel with one lumen of a θ pipette filled with 1% BSA Ringer (washout) and another lumen with 0.75mg/ml TRITC-BSA (dye) in 1% BSA Ringer. When the pressure at the washout side was increased to 30-60 cmH_2O while the pressure at the dye side was 10-15 cmH_2O to balance the pressure from the downstream, the settings were for the perfusion of washout solution. Alternately, when the pressure at dye side was set to 30-60 cm H_2O and that at the washout side to 10-15 cmH_2O, the settings were for the perfusion of dye solution. After the baseline measurement, we recannulated the same vessel with a new θ pipette with one lumen filled with 0.5 mg/ml NaF in 1%BSA Ringer, another lumen filled with 0.75mg/ml TRITC-BSA in 1%BSA Ringer. We first perfused the

vessel with 0.5 mg/ml NaF and simultaneously exposed to 0.37 mW/mm^2 light of 490 nm wavelength for 2-5 min, then switched the light to 540nm wavelength and perfused the vessel with 0.75mg/ml TRITC-BSA to measure *P*. The time taken for an individual *P* measurement was 15-20 sec. *P* was then measured every 5 min thereafter for up to 30 min. To examine *P* change prior to onset of thrombosis, in another group of microvessels, we measured *P* every min from the beginning of the light/NaF treatment up to 10 min. To examine *P* change prior to onset of thrombosis, in another group of microvessels, we measured *P* every min from the beginning of the light/NaF treatment up to 10 min.

To account for the effect from the activated blood cells under light/NaF treatment on *P*, we also measured *P* of the microvessels at the initiation of thrombosis as we did for *Lp*. A θ micropipette with one lumen containing 0.5mg/ml NaF in 1% BSA Ringer and another lumen containing 0.75mg/ml TRITC-BSA in 1% BSA Ringer was used to cannulate the microvessel at the initiation of thrombosis, *P* was measured immediately and then every 5 min after exposure to the light for 20 min.

Measurement of microvascular reflection coefficient σ to albumin

The technique for measuring microvessel reflection coefficient (σ) to a solute was described by Kendall and Michel (1995). Briefly, from Starling's principle,

$$J_V/A = L_P P_c - L_P(\sigma\Delta\pi + P_i) \qquad (1)$$

where, Jv/A is the net fluid flow per unit area of vessel wall, *Lp* is the hydraulic permeability, P_c is the microvascular pressure, $\Delta\pi$ is the oncotic pressure difference between the plasma and interstitial fluid, and P_i is the interstitial fluid pressure. Assuming P_i and $\sigma\Delta\pi$ are constant, Lp is the slope. The intercept on the P_c axis is $\sigma\Delta\pi$ if assuming the interstitial pressure P_i zero. If the perfusate oncotic pressure π_p is known, σ was estimated from $\sigma\Delta\pi$, $\sigma \approx (\sigma\Delta\pi/\pi_p)^{1/2}$ when $Jv/A \geq 0$ (Kendall and Michel, 1995). To measure σ to albumin at control condition, we did two experiments with BSA concentration 1% and 5% with the corresponding oncotic pressures π_p 3.92 and 19.6 cmH_2O respectively. A vessel was cannulated and perfused with 1% (or 5%) BSA Ringer containing red blood cells as marker cells. After a short time of perfusion, the vessel was blocked at the downstream using a glass pipette and the movement of maker cells was recorded. After 10 - 15 s, the vessel was reperfused and the perfusion pressure was reset. This procedure repeated under three perfusion pressures with ~10 cmH_2O increment.

To measure σ to albumin at the onset of thrombosis, a micropipette containing 0.5mg/ml NaF in 1% (or 5%) BSA Ringer was used to cannulate and perfuse a microvessel. After exposure to $0.37mW/mm^2$ light for ~5min, the downstream of the vessel was completely occluded, and the marker cell velocity was recorded. This procedure repeated under three perfusion pressures with ~10 cmH_2O increment. Using this technique, we also measured σ to albumin in the vessels at the thrombosis initiation and in the vessels with 50-75% thrombus occlusion.

Determination of diffusive solute permeability P_d from measured apparent permeability P

Since solute flux can be coupled to water flow (solvent drag), the permeability coefficient *P* measured in our experiments (apparent permeability) tends to overestimate the true diffusive permeability (P_d) of large molecules. Using the hydraulic conductivity *Lp* value of rat mesenteric microvessel measured in previous section 0.983×10^{-7} cm/s/cm H_2O, we calculated the diffusive permeability P_d for TRITC-BSA (the data are summarized in **Table 3.1**) by employing the following formula in (Curry and Frokjaer-Jensen, 1984; Fu *et al.*, 2003; Fu and Shen, 2004),

$$P = P_d \frac{Pe}{\exp(Pe) - 1} + L_p (1 - \sigma)\Delta p_{eff} \tag{2}$$

$$Pe = \frac{Lp(1 - \sigma)\Delta p_{eff}}{P_d} \tag{3}$$

$$\Delta p_{eff} = \Delta p - \sigma^{albumin} \Delta \pi^{albumin} - \sigma^{TRITC-albumin} \Delta \pi^{TRITC-albumin} \tag{4}$$

where *Lp* is the hydraulic conductivity of the microvessel, σ is the reflection coefficient of the microvessel to the solute, and Δp_{eff} is the effective filtration pressure across the microvessel wall. Δp and $\Delta \pi$ are the hydrostatic and oncotic pressure drops across the microvessel wall, respectively. We assumed $\sigma^{albumin} = \sigma^{TRITC-albumin} = \sigma$ in our study.

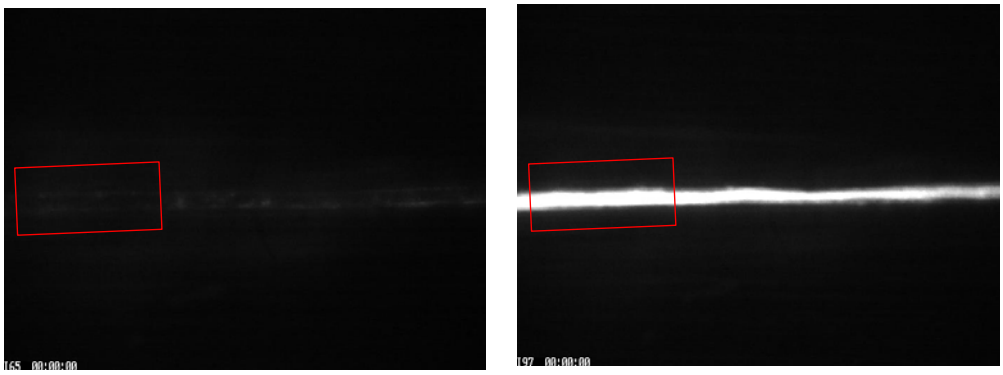

Fig. 3.4 A microvessel before (a) and after (b) filled with the fluorescent solution. The fluorescence intensity in the rectangular window (in red) was measured to determine the solute permeability *P*.

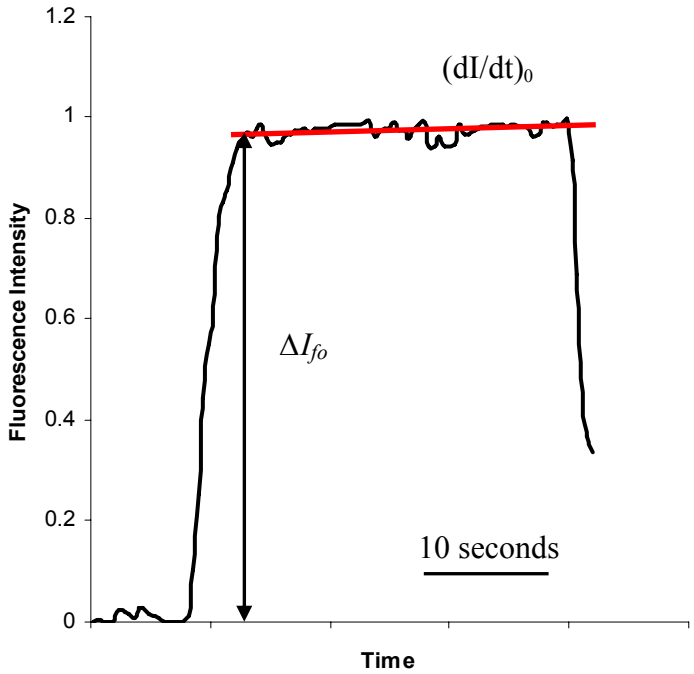

Fig. 3.5 A typical curve of fluorescence intensity (normalized value) as a function of time for solute permeability measurement.

Data analysis and statistics

Microvessel *Lp* or *P* measurements during the control period in a vessel were averaged to establish a single value for a baseline *Lp* or *P*. This value was then used as a reference for all subsequent measurements on that vessel. To present the data at a specific time for the light/NaF effect, *Lp* or *P* was first grouped in 2-5 min after treatment, then individual measurements were grouped at every 5 min (± 2.5 min). The nonparametric Wilcoxon signed rank test was applied to the averaged *Lp* or *P* data to test statistical significance of the treatment over time. Mann-Whitney's U test was applied to between-group data to test *Lp* or *P* differences at specific times. Significance was assumed for probability levels $p < 0.05$. All values were means ± SE, unless otherwise specified.

Results

Light/dye induced microvascular thrombosis

Figure 3.6 shows the thrombus formation induced by light/NaF in a representative microvessel of rat mesentery. Thrombi were initiated ~3 min after the vessel was injected with 10mg/ml NaF at 50 mg/kg body weight and exposed to 490 nm wavelength light (0.37 mW/mm^2) (**Fig. 3.6a**); ~18 min after the treatment, thrombi were formed uniformly on both sides of the vessel and occupied ~60% of the mid-plane area $D \times L$ in the vessel segment (D, vessel diameter; L, length of the vessel segment) (**Fig. 3.6b**); 5 min later, the vessel was ~90% occluded by thrombi (**Fig. 3.6c**). Finally, the vessel was completely blocked after ~28 min light/dye treatment.

Figure 3.7 summarizes thrombus formation as a function of time. The size of thrombus was normalized with *D*L*. At a light intensity of 0.37 mW/mm^2 (■, solid line), thrombi were initiated in 3.8 ± 0.4 (SE, n=8) min after light/dye treatment. An almost linear thrombus growth was found (R^2=0.985) and the average thrombus growth rate was 3.9% ± 0.3% 1/min. The vessels were fully occluded in 29.3 ± 2.2 min. In addition, we tested the effect of light intensity on thrombosis by exposing the vessels to a higher intensity of 0.70 mW/mm^2 (Δ, dashed line). Under this intensity, thrombi were initiated in a shorter time of 2.5 ± 0.35 (SE, n=9) min. The thrombus size vs. time curve was also linear (R^2=0.996) and the average thrombus growth rate was 7.5% ± 1.2% 1/min, and vessels were completely occluded in 15.5 ± 1.8 min. Under both intensities, after vessels were completely occluded, the light was turned off for ~30 min, no thrombi became smaller or disappeared in any of these vessels.

For comparison, we also observed the same type of microvessels in the mesentery, which were perfused with NaF but without exposure to the light. These vessels were > 2 mm away from those exposed to the light. During our 30 min observation, no thrombosis occurred in these vessels (n = 20) under above two light intensities. We also observed those vessels exposed to the light but in the absence of NaF and found no thrombosis in these vessels as well (n =18).

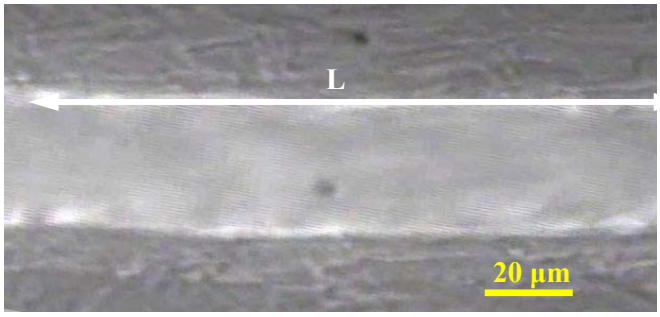

(a) t ~3 min

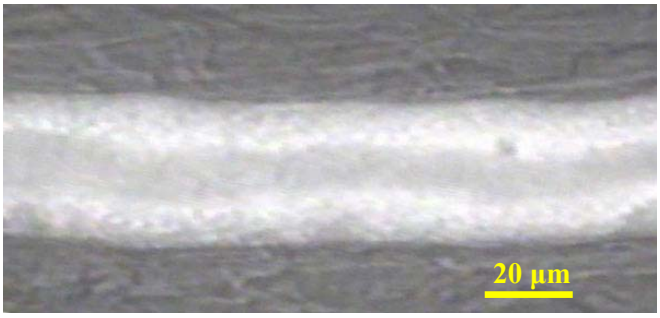

(b) t ~ 18 min

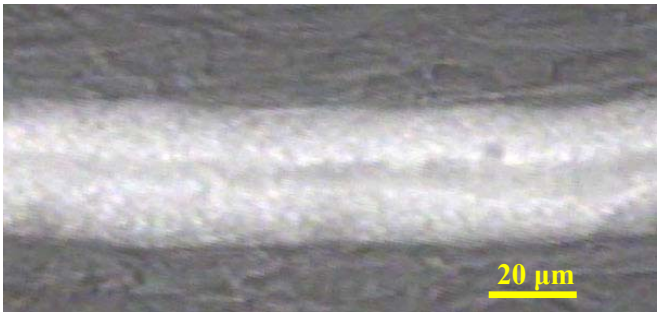

(c) t ~ 23 min

Fig. 3.6 Experimental observations of thrombosis in a post-capillary venule of the rat mesentery. The irradiated light density was 0.37 mW/mm^2. **(a)** Thrombosis started in a microvessel after ~3min exposure to the light of 490 nm wavelength while NaF was injected simultaneously through the carotid artery; **(b)** After 18 min exposure, the bright area represents the thrombi formed from both sides of the vessel wall; **(c)** After 23 min exposure, thrombi occluded most part of the microvessel.

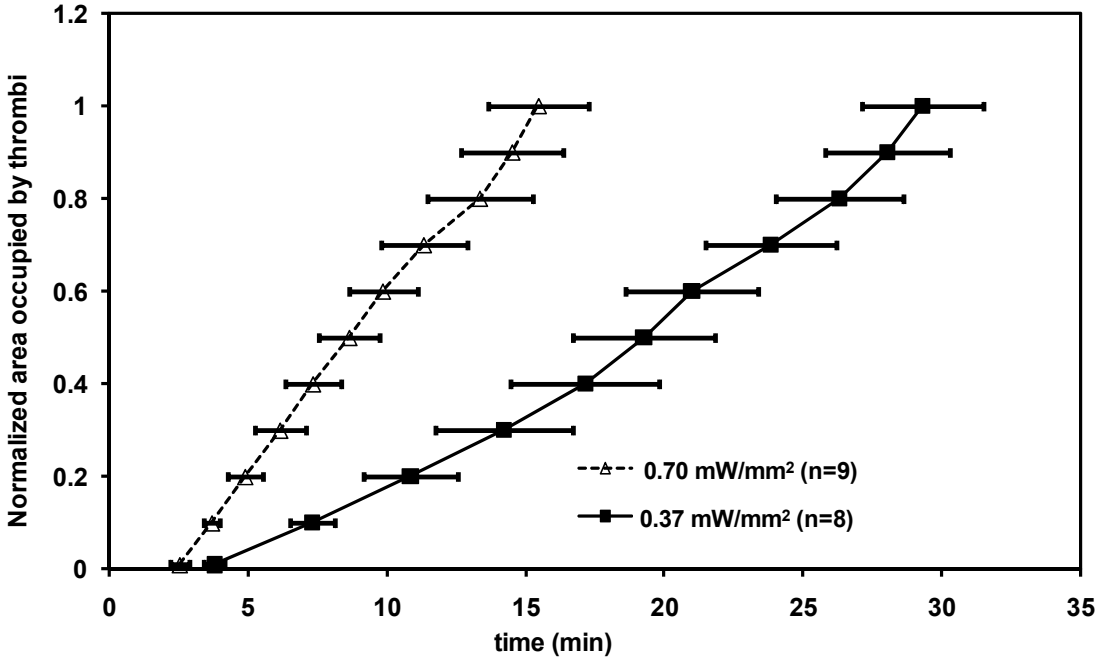

Fig. 3.7 Light/NaF treatment induced thrombus growth as a function of time. The thrombus occupied area was normalized by the plane area of a vessel segment, $D \times L$, where D is the vessel diameter and L the length of the vessel segment. Two irradiation light intensities, 0.37 mW/mm^2 (■, n = 8) and 0.70 mW/mm^2 (Δ, n = 9), were applied. Injected NaF dose was 50mg/kg body weight. Data shown are Mean ± SE.

Microvascular hydraulic conductivity Lp increased by light/dye treatment

To investigate the structural mechanisms of light/dye induced microvascular thrombosis, we measured the change of *Lp* under the same light/dye treatment as for the thrombosis (0.37 mW/mm^2 light intensity and 0.5 mg/ml local NaF concentration). **Figure 3.8a** shows the mean (± SE) *Lp* relative to its baseline value as

a function of time for control and test experiments. After vessels were treated with 0.5 mg/ml NaF and 0.37 mW/mm^2 light (■, solid line) for 2-5 min, average 3.5 ± 0.3 min (SE, n=11), which was the same timing for thrombus initiation, *Lp* increased 2.2 ± 0.2 folds from its mean baseline value (*p < 0.001). Longer time (up to 30 min) treatment did not further increase *Lp* (p > 0.7). Five min after the light was turned off, *Lp* became 1.6 ± 0.2-fold of the baseline *Lp* (# p = 0.013), which was an insignificant decrease from that after 30 min treatment (p = 0.4). For comparison, when vessels were exposed to 0.37 mW/mm^2 light alone (□, dotted line, n = 4) or treated with 0.5 mg/ml NaF alone (Δ, dashed line, n = 4), *Lp* did not change significantly from the baseline (p >0.3). The sham control experiment (×, dash-dot-dash line, n = 4) showed that micropipette recannulation or solution reperfusion would not change *Lp* significantly (p = 0.36).

Figure 3.8b summarizes the mean (± SE) values for *Lp* in control and test experiments. In 3.5 ± 0.3 min (SE, n=11) after light/NaF treatment, *Lp* increased significantly from a mean of 0.98 (± 0.08, range: 0.69 – 1.52) to 2.07 (± 0.21, range: 1.11 – 3.16) × 10^{-7} cm/s/cmH_2O (*p < 0.001). No further increase occurred after longer time treatment (up to 30 min). Five min after light was turned off, *Lp* insignificantly decreased to 1.64 (± 0.19, range: 1.01 – 2.53) × 10^{-7} cm/s/cmH_2O (p = 0.4 compared with light on). But this *Lp* was significantly higher than the baseline (# p = 0.013 compared with baseline). No further change in *Lp* occurred 20 min after light off. Comparison of *Lp* under the light/dye treatment with those either treated with the light alone, or treated with 0.5 mg/ml NaF alone, or the sham control due to

surgical processes, we found that *Lp* under the light/dye treatment increased significantly (*$p < 0.001$); the difference was significant even after the light was turned off (#$p < 0.015$).

To investigate *Lp* change prior to onset of thrombosis, we measured *Lp* from the beginning of the light/NaF treatment. **Fig. 3.8c** demonstrates that after 1 min light/dye treatment, *Lp* significantly increased to 1.2 ± 0.1 folds ($n = 6$) of its baseline ($p = 0.0027$). Compared to 1 min treatment, 2 min treatment further increased *Lp* to 1.4 ± 0.2 folds of the baseline ($p = 0.03$). Three min treatment increased *Lp* to 1.7 ± 0.2 folds, which was significant from 2 min treatment ($p = 0.04$). However, 4 min treatment increased *Lp* to 2.1 ± 0.2 folds, which was not significant from the increase at 3 min ($p = 0.11$). Five min or longer treatment did not increase *Lp* further from the 4 min treatment ($p > 0.8$).

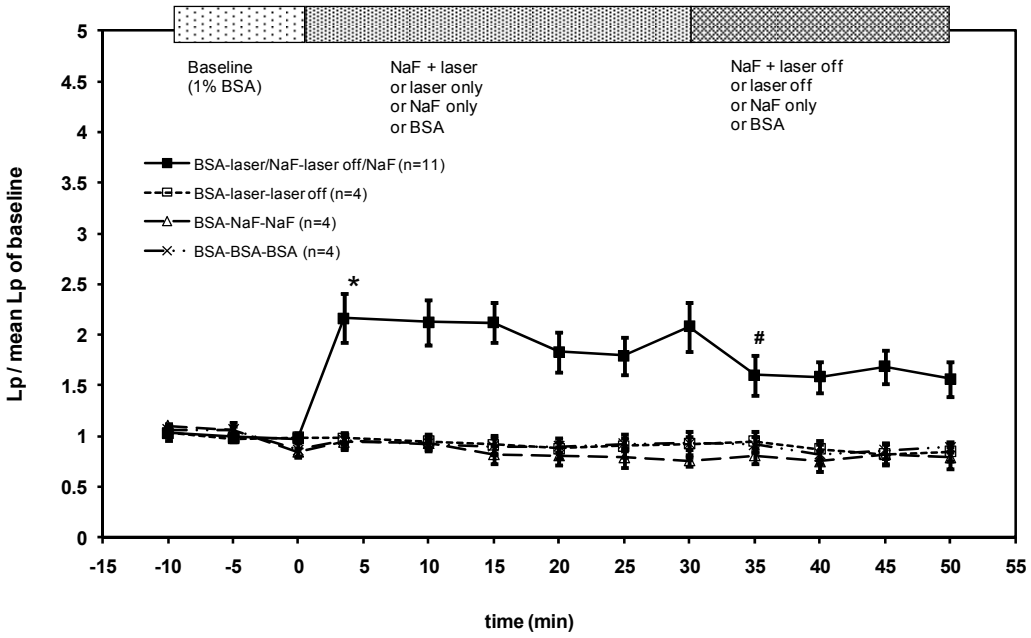
Baseline
(1% BSA)
NaF + laser
or laser only
or NaF only
or BSA
NaF + laser off
or laser off
or NaF only
or BSA
BSA-laser/NaF-laser off/NaF (n=11)
BSA-laser-laser off (n=4)
BSA-NaF-NaF (n=4)
BSA-BSA-BSA (n=4)
Lp / mean Lp of baseline
time (min)

(a)

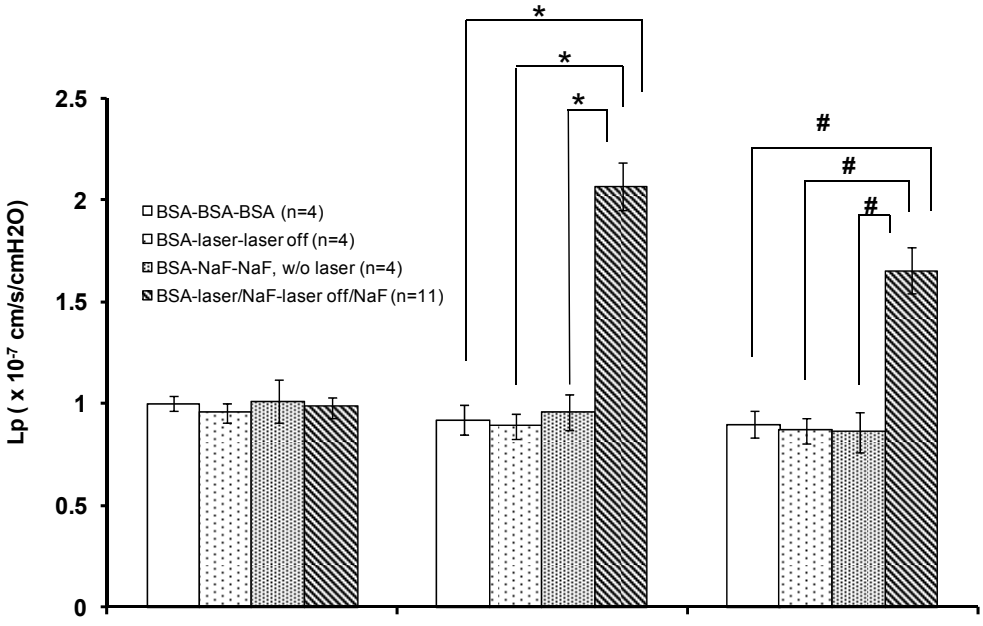
BSA-BSA-BSA (n=4)
BSA-laser-laser off (n=4)
BSA-NaF-NaF, w/o laser (n=4)
BSA-laser/NaF-laser off/NaF (n=11)
Lp (x 10-7 cm/s/cmH2O)

(b)

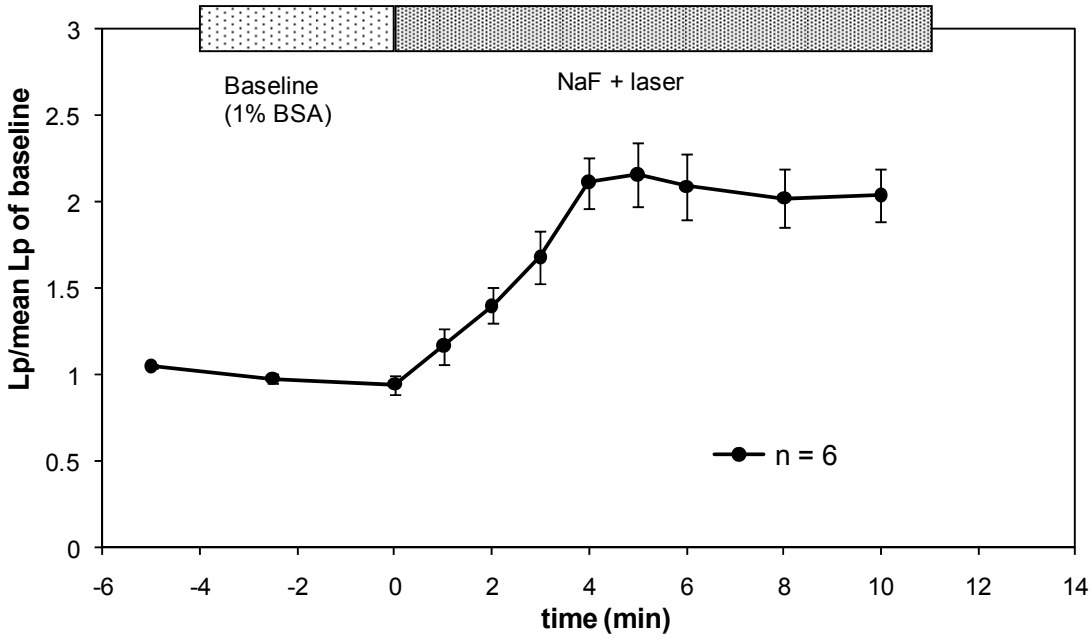

(c)

Fig. 3.8 (a) Normalized hydraulic conductivity *Lp* by the mean baseline value as a function of time. In the various control groups, baseline *Lp* was first measured with Ringer perfusate containing 1% BSA, then *Lp* was measured 1) when the vessel was exposed to the laser in the absence of NaF for 30 min and laser off for another 20 min (□, BSA-laser-laser off, n = 4); 2) in the presence of 0.5 mg/ml NaF and without exposure to the laser for 50 min (Δ, BSA-NaF-NaF, n = 4); and 3) in the absence of NaF and without exposure to the laser for 50 min (×, BSA-BSA-BSA, n = 4). In the test group (■, BSA-laser/NaF-laser off/NaF), baseline *Lp* was measured first with Ringer perfusate containing 1% BSA, then *Lp* was measured in the presence of 0.5 mg/ml NaF and exposure to the laser (0.37 mW/mm^2) for 30 min, and finally *Lp* was measured for another 20 min after the laser was turned off. *$p < 0.001$ and #$p < 0.01$, compared with the baseline value. Data shown are Mean ± SE. **(b)** Comparison of *Lp* at the baseline, after 2-5 min laser/NaF treatment, and 5 min after laser off, with its values under various sham controls. *$p < 0.001$ and #$p < 0.015$. . **(c)** At early time after exposure to the light. * $p < 0.001$ and #$p < 0.003$, compared with the baseline value. Data shown are Mean ± SE.

Microvascular solute permeability P increased by light/dye treatment

To find out the most likely structural mechanisms by which the light/dye induced thrombosis, we also measured the microvessel solute permeability *P* to TRITC-BSA under the same light/dye treatment as for the thrombosis and the *Lp*. **Figure 3.9a** shows the mean microvessel $P^{albumin}$ (± SE) relative to its baseline value as a function of time in control and test experiments. After vessels were treated with 0.5 mg/ml NaF and 0.37 mW/mm^2 light for 2-5 min, average 3.7 ± 0.3 min (SE, n=7), which was the same timing for thrombus initiation, $P^{albumin}$ increased from the mean baseline value 8.37 (± 0.88) × 10^{-7} cm/s to 34.6 (± 5.3) × 10^{-7} cm/s (*$p < 0.015$), a 4.1 ± 0.7-fold increase. Longer time (up to 30 min) light/NaF treatment did further increase *P* ($p > 0.4$, later times compared to that after 2-5 min treatment).

As for *Lp*, to investigate *P* change prior to onset of thrombosis, we measured *P* from the beginning of the light/NaF treatment. **Figure 3.9b** demonstrates that after 1 min light/dye treatment, *P* significantly increased to 2.0 ± 0.2 folds ($n = 6$) of its baseline ($p = 0.0014$). Compared to 1 min treatment, 2 min treatment further increased *P* to 3.0 ± 0.3 folds of the baseline ($p = 0.04$). Three min treatment increased *P* to 4.1 ± 0.4 folds, which was significant from 2 min treatment ($p = 0.03$). However, 4 min treatment increased *P* to 4.2 ± 0.4 folds, which was not significant from the increase at 3 min ($p = 0.2$). Five min or longer treatment did not increase *Lp* further from the 4 min treatment ($p > 0.8$).

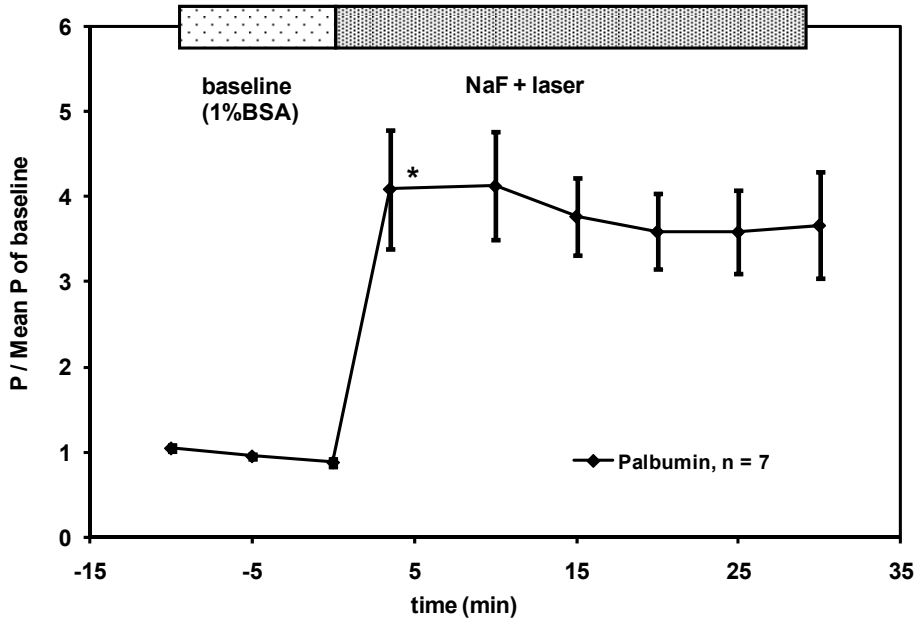

(a)

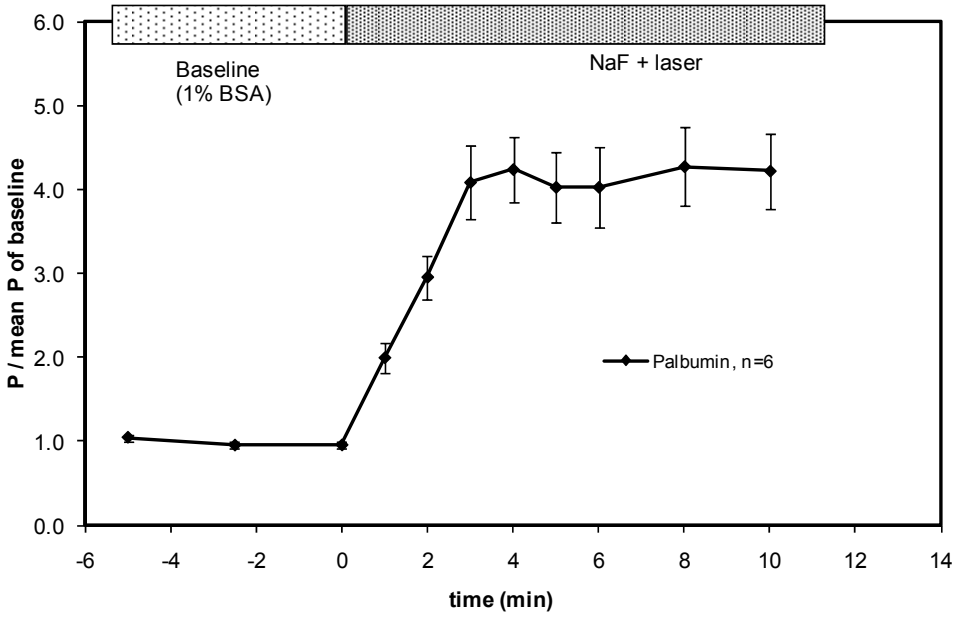

(b)

Fig. 3.9 Normalized solute permeability $P^{albumin}$ as a function of time. **(a)** Baseline P was measured first with Ringer perfusate containing 1% BSA, then P was measured in the presence of 0.5 mg/ml NaF and exposure to the laser (0.37 mW/mm^2) for 30 min * $p < 0.003$ compared to the baseline value. **(b)** At early time after exposure to

the light. * $p < 0.001$ and # $p < 0.003$, compared with the baseline value. Data shown are Mean ± SE.

Comparison of microvascular permeability increase under light/dye treatment in the presence and absence of blood cells

To investigate the contribution from activated blood cells under the light/dye treatment to microvascular permeability increase, we also measured *Lp*/*P* in the vessels at the initiation of thrombosis and when the vessels were 50-75% occluded by the thrombi. In **Fig. 3.10**, the line with ♦ is the result in the absence of blood cells; the line with ■ is for that after thrombosis initiation; and the line with ▲ is for that after partial occlusion. **Figure 3.10a** shows that at the initiation of thrombosis after 4.2 ± 0.4 min light/dye treatment, *Lp* increased to 2.5 ± 0.3 folds of its baseline (n = 9), which was not significant from the 2.2 ± 0.2 fold increase after 3.5 ± 0.3 min light/dye treatment in the absence of blood cells (n = 11) (p = 0.86). *Lp* measured when the vessels were 57% ± 4% occluded after 21.2 ± 2.4 min treatment was 2.6 ± 0.3 folds of its baseline, which was insignificant from that (1.8 ± 0.2 folds of the baseline) measured after 20.0 ± 2.5 min treatment in the absence of blood cells (p = 0.11). Similarly, **Fig. 3.10b** shows that at the initiation of thrombosis after 4.6 ± 0.3 min light/dye treatment, *P* increased to 4.3 ± 0.5 folds of its baseline (n = 6), which was not significant from the 4.1 ± 0.7 fold increase after 3.7 ± 0.3 min light/dye treatment in the absence of blood cells (n = 7) (p = 0.72).

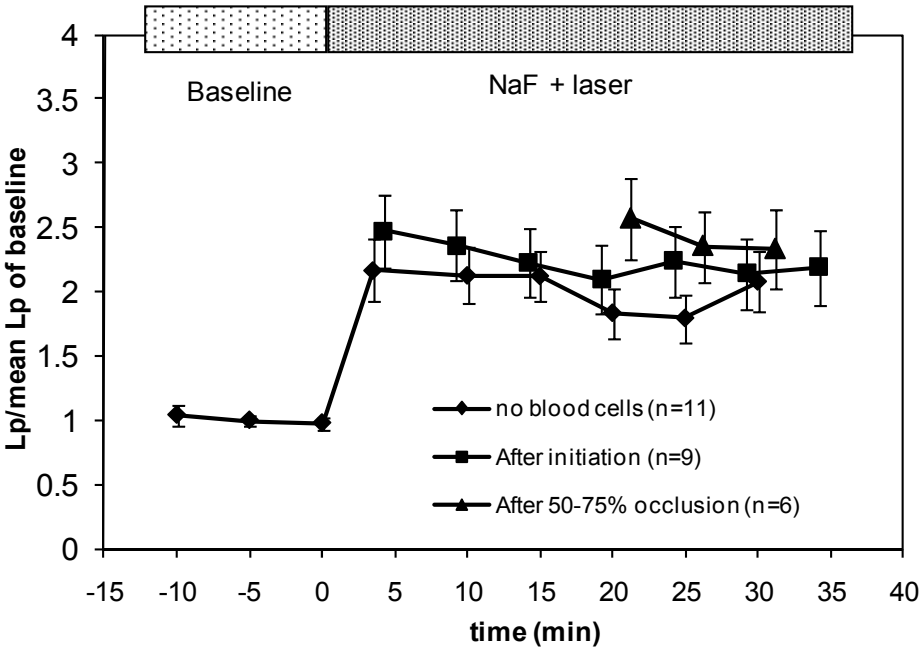

(a)

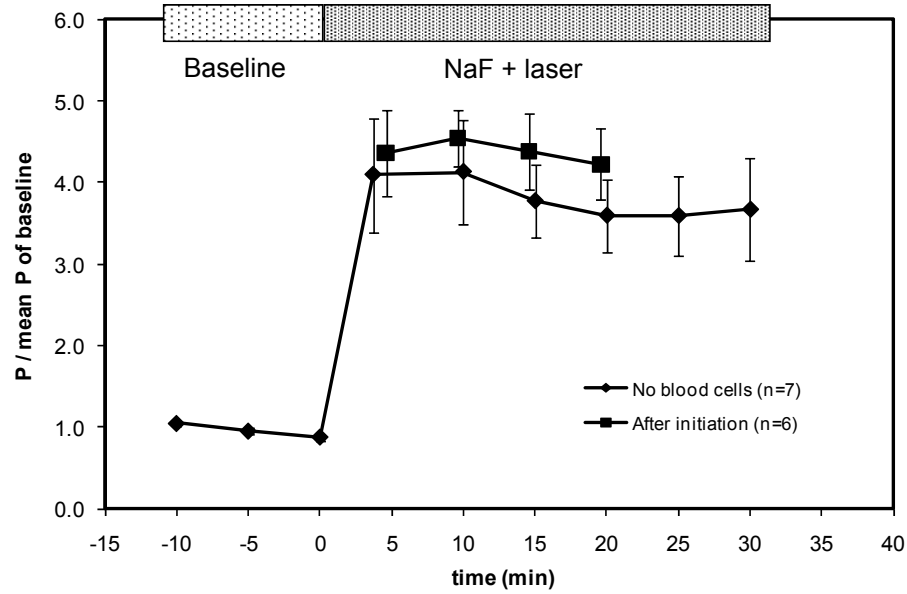

(b)

Fig. 3.10 Comparison of permeability increase under the light/dye treatment in the absence of blood cells (♦), at the initiation of thrombosis (■), and after the vessels were 50-75% occluded by thrombi (▲). **(a)** *Lp*; **(b)** *P* to albumin.

Microvascular reflection coefficient σ to albumin decreased by light/dye treatment

Since the microvascular reflection coefficient σ to albumin is a measure for selectivity of the microvessel wall, which also contributes to the solvent drag component (convection) of apparent permeability of albumin (measured *P*), it was thus determined under the same light/dye treatments for thrombosis and *Lp/P* measurement. **Figure 3.11** plots the estimation of $\sigma\Delta\pi$ vs. the corresponding oncotic pressure π_p for the experiments. **Figure 3.11a** is under control experiments, and **Fig. 3.11b** is after approximately 5 min light/dye treatment. Under control measurement $\sigma\Delta\pi = 0.152 + 0.794\pi_p$, while after light/dye treatment $\sigma\Delta\pi = 0.440 + 0.397\pi_p$. Since the reflection coefficient σ of vessel wall to albumin is $(\sigma\Delta\pi/\pi_p)^{1/2}$ (Kendall and Michel, 1996), our experiments found after 4.7 ± 0.3 min light/dye treatment in the absence of blood cells, σ to albumin decreased from 0.89 at baseline to 0.63; at the initiation of thrombosis after 4.2 ± 0.3 min light/dye treatment in the presence of blood cells, σ to albumin was 0.48 ± 0.03 (n = 6); when the microvessels were 50-75% occluded after 22.2 ± 1.5 min light/dye treatment, σ to albumin was 0.46 ± 0.06 (n = 6). There was no significant difference in σ to albumin under these three conditions ($p > 0.15$).

In our experiment, Δp ranges 10 - 20 cm H_2O, by assuming Δp 15 cm H_2O, Δp_{eff} is 11.27 cm H_2O, $\sigma^{albumin}$ was 0.89 from our experiments and $\Delta\pi^{albumin}$ were 3.92 cmH_2O respectively for 1% BSA, $\Delta\pi^{TRITC\text{-}albumin}$ was 0.27 cm H_2O for 0.75 mg/ml TRITC-BSA, $\sigma^{TRITC\text{-}albumin}$ were to be 0.89 and 0.63. Using these parameters, the

diffusive permeability of albumin $P_d^{albumin}$ was calculated as 0.84×10^{-6} cm/s, which was 93% of its apparent permeability. Under light/dye treatment, the solvent drag contributed to $P^{albumin}$ 14% when Δp_{eff} = 12.36 cm H_2O when $\sigma^{albumin}$ decreased to 0.63 (**Table 3.1**).

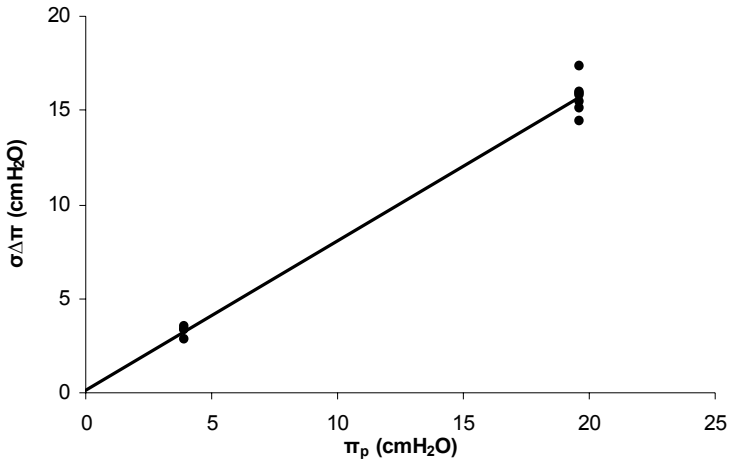

(a)

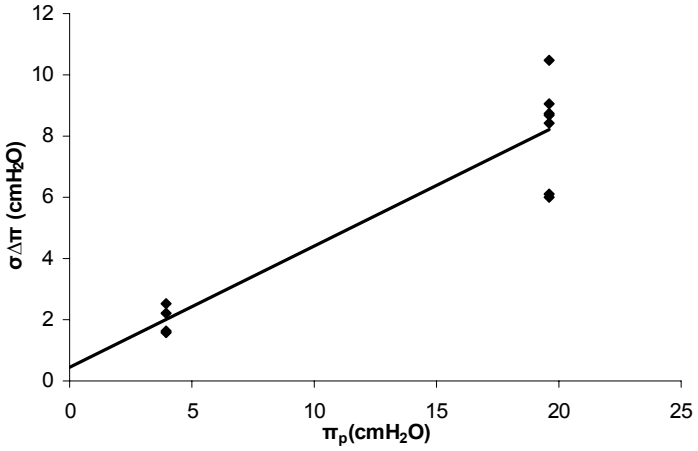

(b)

Fig. 3.11 The relation between perfusate oncotic pressure π_p and $\sigma\Delta\pi$. (a) under control; (b) after ~ 5 min light-dye treatment.

Table 3.1 Solvent drag effect on BSA permeability under control and light/dye treatment

Δp_{eff} (cm H_2O)		Lp (cm/s/cmH_2O)	P (x 10^{-6} cm/s)	Pe	P_d (x 10^{-6} cm/s)	P_d/P
Control						
11.27	$\sigma^{albumin} = 0.89$	0.98 x 10^{-7}	0.84	0.16	0.77	0.93
Light-dye						
12.36	$\sigma^{albumin} = 0.63$	2.07 x 10^{-7}	3.46	0.32	2.96	0.86

Model predictions

To predict microvascular permeability increase by compromising the integrity of interendothelial cleft, we adopted the mathematical model developed by Fu *et al.* (1994). The model geometry is shown in **Fig. 3.1**. Under normal physiological conditions, electron microscopy study on rat mesenteric microvessels (Adamson *et al.*, 2004) revealed that on average, the cleft width $2B$ = 18 nm, large break width $2d$ = 315 nm, spacing between adjacent large breaks $2D$ = 3590 nm, cleft depth L = 411 nm, and the surface glycocalyx thickness L_f = 150 nm. The glycocalyx fiber radius a = 6 nm, and gap spacing between fibers Δ = 8 nm (Squire *et al.*, 2001). Our predictions for the permeability increase were based on these baseline parameters. **Figure 3.12** shows our model predictions for increasing Lp and $P^{albumin}$ by changing the structural components of the interendothelial cleft. If the light/dye degrades the surface glycocalyx (decreasing L_f), $P^{albumin}$ would increase largely while Lp only have moderate increase (**Fig. 3.12a**); if the light/dye increases the gap ($2B$) between endothelial cells (endothelial cells contract or shrink), Lp would increase greatly

while $P^{albumin}$ have a moderate increase (**Fig. 3.12b**); if the light/dye increases the size (*2d*) (**Fig. 3.12c**) or number (decreasing *2D*) (**Fig. 3.12d**) of junctional pores in the cleft, *Lp* would have a moderate increase while $P^{albumin}$ only a negligible increase. We also used L_f = 400 nm, which is an averaged value measured in the microvessels of hamster or mouse cremaster muscles by *in vivo* microparticle image velocimetry or observation of a exclusion zone of fluorescence-labeled macromolecules (Vink and Duling, 1996; Smith *et al.*, 2003; Damiano *et al.*, 2004). The predicted patterns for structural changes vs. *Lp/P* were similar to those when L_f = 150 nm. However, using L_f = 150 nm would give values of *Lp* and *P* comparable to the measured data, while L_f = 400 nm would give values of *Lp* and *P* too low.

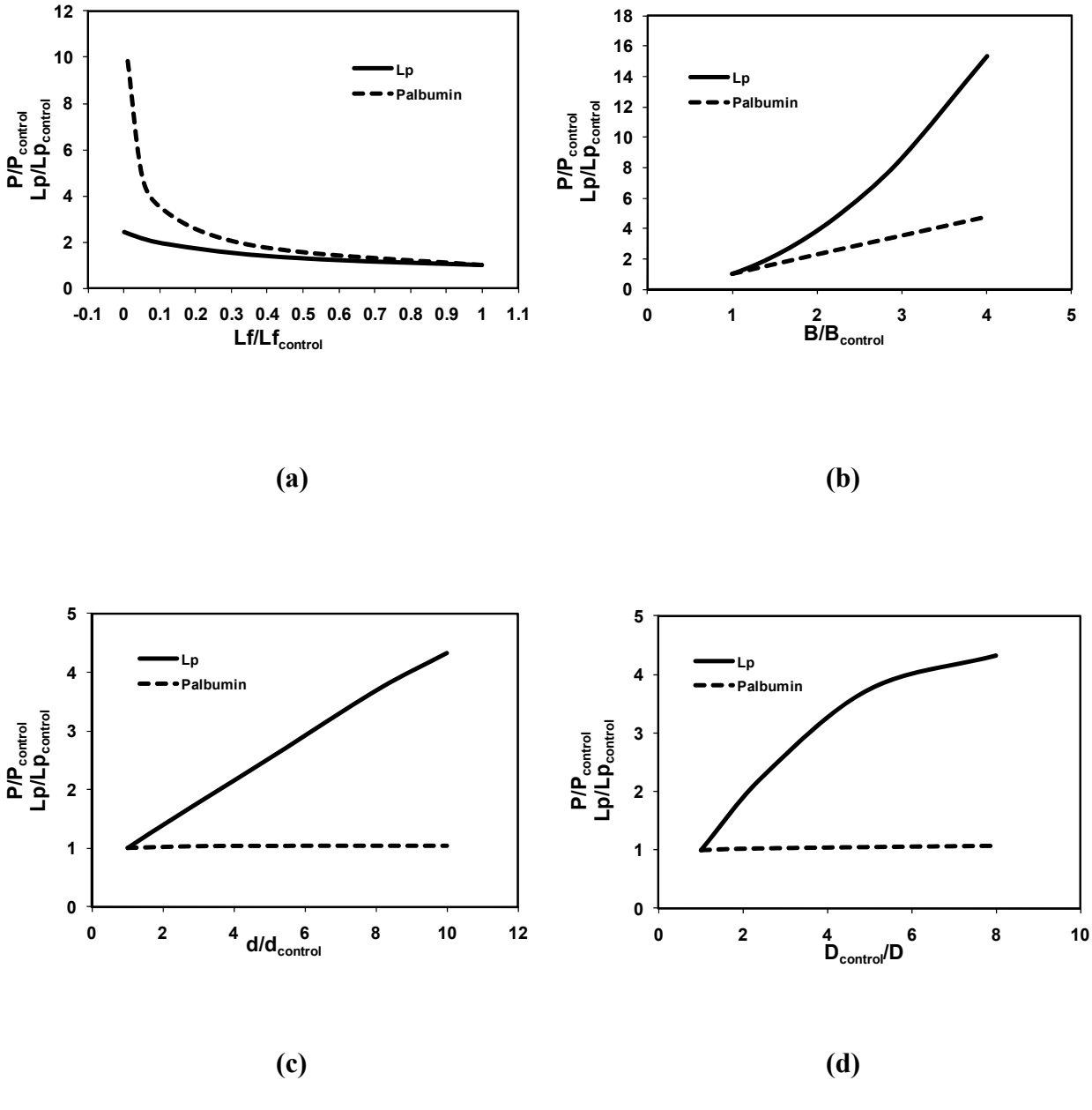

Fig. 3.12 Model predictions for the effect of changing structural components of the interendothelial cleft on *Lp* and *P* of albumin. **(a)** Decreasing the surface glycocalyx thickness L_f; **(b)** increasing the cleft width *2B*; **(c)** increasing the junctional break width *2d*; **(d)** increasing the number of junctional breaks.

Discussion

In both *ex vivo* and *in vitro* models, Chen *et al.* (2006) observed endothelial cell barrier damage following PDT, where endothelial cells retract, leading to the formation of intercellular gaps. Michels *et al.* (2003) found that PDT in humans with classic choroidal neovascularization (CNV) caused vascular barrier dysfunction, and hypothesized that the increase of leakage was due to the damage to vascular endothelial cells and pericytes of the CNV and normal choriocapillary network. Proske *et al.* (2000) found massive extravasation of macromolecules after induction of micro-venular thrombosis in mouse skin, suggesting the loss of endothelial integrity. Previous studies also found that light/dye treatment can induce microvascular thrombosis in a variety of tissues and species in the absence of endothelial denudation or injury (summarized in Rumbaut *et al.*, 2005). For example, using light and electron microscopy, Miller *et al.,* (1992) found that after 10 min light/dye treatment under a low irradiation power of 2 mW/mm^2, macromolecular leakage and platelet activation were observed in venules (30-40 μm diameter) of rat cremaster muscles with no increase in vessel diameters and visible structural damages. In contrast, 60 min light/dye treatment under this power induced endothelial and smooth muscle swelling and rupture, gap formation and accumulation of leukocytes at the vessel walls. Povlishock *et al.,* (1983) observed subtle endothelial abnormalities at the onset of platelet aggregation in cat pial microvessels under light/dye treatment. These abnormalities included vacuolization of the endothelium, increased endothelial lucency, swelling of the nuclear envelope, and rupture of the

luminal membrane. However, more subtle structural changes may be induced in microvascular endothelium, especially at a low power of PDT or light/dye treatment.

In the present study, we wanted to investigate these more subtle structural changes in the microvessel by the light/dye that increased microvascular permeability and induced thrombosis. The possible changes for *Lp* and *P* to albumin are predicted in **Fig. 3.13** upon changing the structural components of the inter-endothelial cleft. After correcting for the solvent drag due to the filtration across the microvessel wall, the ratio of diffusive permeability to albumin under light/dye treatment in the absence of blood cells to that under control was 1.7 ± 0.2, 2.7 ± 0.3, 3.8 ± 0.3, 3.9 ± 0.4 and 3.6 ± 0.4 (n = 6) after 1, 2, 3, 4, 5 min treatment, respectively. This ratio was 3.6 ± 0.3 (n = 6) at the initiation of thrombosis. In parallel, the ratio of *Lp* under light/dye treatment in the absence of blood cells to that under control was 1.2 ± 0.1, 1.4 ± 0.2, 1.7 ± 0.2, 2.1 ± 0.2 and 2.2 ± 0.2 (n = 6) after 1, 2, 3, 4, 5 min treatment, respectively. It was 2.5 ± 0.3 (n = 9) at the initiation of thrombosis. Comparing these measured *Lp* and *P* data with the model predictions for *Lp* and *P* changes when degrading the endothelial surface glycocalyx in **Fig. 3.13**, we could find that if normal L_f = 150 nm, the light/NaF treatment for 1,2,3,4,5 min would degrade the glycocalyx layer by 33-50%, 60-77%, 80-90%, 92-94% and 91-95%, respectively; if normal L_f = 400 nm, these ratios were 30-40%, 54-76%, 70%, 84-85%, and 85%, respectively. Our results are consistent with the previous observation that the light/dye treatment degraded the glycocalyx in mouse and hamster cremaster microvessels (Smith *et al.*, 2003; Damiano *et al.*, 2004; Vink and Duling, 1996). In contrast, all other structural

changes, e.g. increasing the gap between endothelial cells and increasing the size and number of junction breaks would result a larger relative increase in *Lp* than that in *P* to albumin, and thus do not reconcile with our measured data.

Figures 3.8c and **3.9b** demonstrate that prior to onset of thrombosis, *Lp* and *P* to albumin increased gradually under the light/NaF treatment until reached a plateau in 3-5 min, which was just the timing for thrombosis initiation under our irradiation power. The increased *Lp* and *P* values measured at the thrombosis initiation were also not significantly different from these plateau values in the absence of blood cells. At this timing, **Fig. 3.13** predicts that 92-94% (when L_f =150 nm) or 84-85% (when L_f = 400 nm) of the surface glycocalyx would be degraded, suggesting that the light/dye induced microvessel thrombosis occurs when the surface glycocalyx is almost completely removed. Miller *et al.,* (1992) reported the macromolecular leakage and protein extravasation without thrombosis under their light/dye treatment. Vink and Duling (1996) also observed that no tendency for platelet adhesion during the time that capillary tube hematocrit increased to its maximum value. One possible reason for no thrombosis when macromolecular leakage occurred and no platelet adhesion at the maximum capillary tube hematocrit is that the irradiation was not enough to deplete the glycocalyx to a critical threshold for thrombosis or platelet adhesion. Our observation is consistent with their report. Under our irradiation power, significant glycocalyx (30-50%) was removed even after 1 min light/dye treatment. However, thrombosis was not initiated until longer time treatment. Another possible reason is that the capillaries (~5 μm diameter) in Vink and Duling's experiments are less

susceptible to platelet adhesion than the post-capillary venules (30-50 μm diameter) in the current study.

An interesting observation in our rat mesenteric microvascular thrombosis is that the formation of thrombus was uniform along the vessel wall and at the same rate on both sides of the wall (**Fig. 3.6**). If the light/dye degrades the surface glycocalyx and increases *Lp*, the increased radial fluid flow across the microvessel wall would bring platelets and leukocytes closer to the proximity of the wall and enhance the opportunity of their binding to endothelium. In addition, removing the surface glycocalyx would expose endothelium for the binding. Therefore, degrading the surface glycocalyx by the light/dye could also reconcile with our observation for the uniform formation of thrombus from both sides of the microvessel wall.

To further test if the light/dye induced microvascular thrombus growth rate is correlated with the increased but stable *Lp* and *P* to albumin after the onset of thrombosis, in **Fig. 3.14** we compared the curve of thrombus growth rate vs. time with those of *Lp* vs. time and *P* to albumin vs. time under the similar light/dye treatment. The correlation coefficients are 0.98 and 0.99, respectively, indicating that light/dye induced thrombus growth rate is highly correlated with the stable increased microvessel permeability. The radial fluid flow due to an almost constant increased *Lp* after onset of thrombosis continuously carries the same amount of blood cells to the vessel wall in a given time, inducing a constant thrombus growth rate.

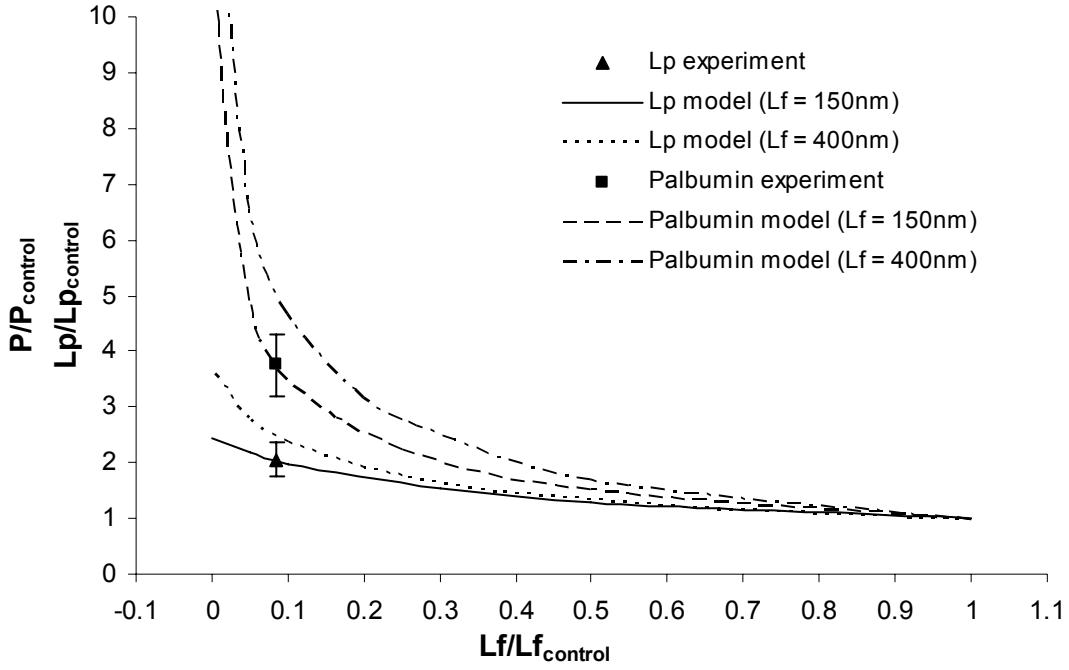

Fig. 3.13 Comparison of experiment results with model predictions of decreasing fiber matrix thickness L_f.

Sato and Ohshima (1984, 1990) used light intensity from 2.4 – 20.7 mW/mm^2 to induce microvascular thrombosis in rat mesenteries and demonstrated that thrombus formation was in proportion to the light intensity and NaF concentration. Interestingly, using the same NaF concentration (50mg/Kg body weight) as in their studies, we found that the thrombus growth rate of 7.5% 1/min, induced by 0.7 mW/mm^2 intensity, and that of 3.9% 1/min, induced by 0.37 mW/mm^2 intensity are exactly proportional to the applied light intensities. In contrast, the initiation and the occlusive times are almost in reverse proportion to the applied intensities.

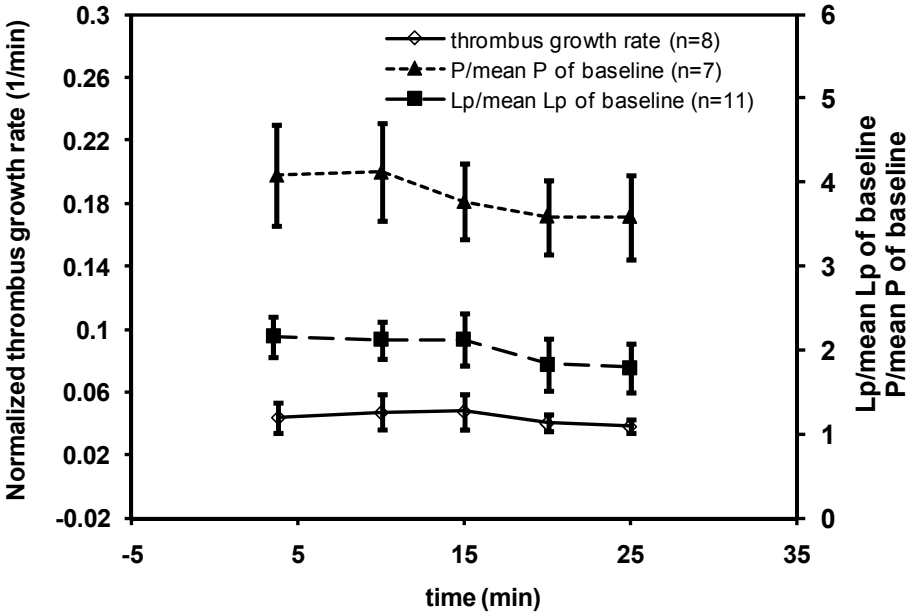

Fig. 3.14 Comparison of time histories of thrombus growth rate, hydraulic conductivity *Lp*, and solute permeability *P* of TRITC-albumin under the light/dye treatment. Data shown are Mean ± SE.

Rumbaut *et al.,* (2004) found that under a light power of 7.7 mW/mm^2, vasoconstriction occurred in arterioles but not in venules of mouse cremaster muscles. Under our much lower light intensity, we found that the diameter of rat mesenteric post-capillary venules has a negligible fluctuation of less than 3%. Previous studies showed that if the light intensity is less than 2 mW/mm^2, hyperthermia would not contribute to thrombosis (Leunig *et al.,* 1994). To confirm this, we measured the temperature in the light/dye solution at 37^{0}C under 0.7 mW/mm^2 and found negligible

fluctuation compared with that without light/dye treatment during 30 min measurement.

CHAPTER 4 SUMMARY AND FUTURE STUDY

Thrombosis can be fatal if it occurs in the brain, in the heart, or in the lung. In the current study, we first investigated the mechanical factors that induce thrombosis using *in vivo* experiments and the 3-D numerical simulation. The experiments revealed that thrombosis occurs at the inner wall of bent/stretched microvessels, while the numerical simulation demonstrated that there are higher shear stresses/rates and higher shear stress/rate gradients at the inner wall, suggesting that localized higher shear stresses/rates and their gradients are the mechanical factors that induce thrombosis in the microvasculature with non-disturbed laminar blood flows.

In the current study, we have found the correlation between thrombosis and the size and bending angle of post-capillary venules, but rather qualitatively. One future study is to quantitatively investigate the effect of localized shear stresses/rates on the initiation time, the growth rate and the size of thrombi. Many previous studies have quantified the flow fields around cells and the cell movements in a circular tube or in between two parallel plates (summarized in Sugihara-Seki and Fu, 2005), but all of them are in straight vessels or chambers. Another future study is thus to simulate blood cell movements in curved/branched microvessels under various laminar flow conditions.

The second part of the study quantified the light/dye induced microvascular thrombosis and microvascular hyperpermeability under a low power irradiation. The results showed that the light/dye treatment gradually increased the microvascular

permeability to a plateau value. The thrombosis was not initiated until the microvascular permeability reached its plateau. A mathematical model predicted that the plateau values for the hydraulic conductivity and solute permeability to albumin correspond to 84-94% degradation of the endothelial surface glycocalyx, suggesting that an almost complete depletion of the surface glycocalyx is the most likely structural mechanism by which the light/dye treatment induces microvascular hyperpermeability and thrombosis.

A detailed observation from the electron microscopy is expected to confirm our predictions for the glycocalyx degradation. This can be one future study. Berman (1953) investigated two-dimensional (2-D) laminar flow in a porous channel with rectangular cross section by using perturbation method. Later on 3-D numerous studies have been conducted on flows in porous tubes or channels (White *et al.* 1958, 1962; summarized in Sugihara-Seki and Fu, 2005). However, no cells were considered in these studies. Therefore, another future study is to quantitatively examine the flow velocity, normal and shear forces on the cells, and the cell movements in the straight and curved microvessels with the permeable walls.

BIBLIOGRAPHY

Adamson, R.H., 1990. Permeability of frog mesenteric capillaries after partial pronase digestion of the endothelial glycocalyx. J Physiol 428, 1–13.

Adamson, R.H., Lenz J.F., Zhang X., Adamson G.N., Weinbaum S., Curry F.E., 2004. Oncotic pressures opposing filtration across non-fenestrated rat microvessels. J Physiol 557, 889–907.

Baker, M., Wayland, H., 1974. On-line volume flow rate and velocity profile measurement for blood in microvessels. Microvasc Res 7 (1), 131–143.

Barker, A.L., Konopatskaya, O., Neal, C.R., Macpherson, J.V., Whatmore, J.L., Winlove, P.C., Unwin, P.R., Shore, A.C., 2004. Observation and characterisation of the glycocalyx of viable human endothelial cells using confocal laser scanning microscopy. Phys Chem Chem Phys 6, 1006–1011.

Berman, A.S., 1953. Laminar flow in channels with porous walls. J Appl Phys 24, 1232–1235.

Begent, N., Born, G.V., 1970. Growth rate in vivo of platelet thrombi, produced by iontophoresis of ADP, as a function of mean blood flow velocity. Nature 227, 926–930.

Bode, L., Murch, S., Freeze, H.H., 2006. Heparan sulfate pays a central role in a dynmaic in vitro model of protein-losing enteropathy. J Biol Chem 281, 7809-7815.

Chappell, D., Jacob, M., Paul, O., Rehm, M., Welsch, U., Stoeckelhuber, M., Conzen, P., Becker, B.F., 2009. The glycocalyx of the human umbilical vein endothelial cell: An impressive structure ex vivo but not in culture. Circ Res 104, 1313–1317.

Chen, J., Lu, X., 2004. Numerical investigation of the non-Newtonian blood flow in a bifurcation model with a non-planar branch. J Biomech 37, 1899–1911.

Chen, B., Pogue B.W., Luna J.M., Hardman R.L., Hoopers P.J., Hasan T., 2006. Tumor vascular permeabilization by vascular-targeting photosensitization: effects, mechanism, and therapeutic implications. Clin Cancer Res 12, 917–923.

Chien, S., 1970. Shear dependence of effective cell volume as a determinant of blood viscosity. Science 168, 977–979.

Chien, S., Usami, S., Taylor, H.M., Lundberg, J.L., Gregersen, M.I., 1966. Effects of hematocrit and plasma proteins on human blood rheology at low shear rates. J Appl Physiol 21, 81–87.

Curry, F.E., 1984. Mechanics and thermodynamics of transcapillary exchange. In: Handbook of Physiology, The Cardiovascular System, Microcirculation (E Renkin, C Michel, Eds.). Bethesda, Maryland. 309–374.

Curry, F. E., Frokjaer-Jensen, J., 1984. Water flow across the walls of single muscle capillaries in the frog, Rana pipiens. J Physiol. 350, 293–307.

Dai, G., Tsukurov, O., Orkin, R.W., Abbott,W.M., Kamm, R.D., Gertler, J.P., 2000. An in vitro cell culture system to study the influence of external pneumatic compression on endothelial function. J Vasc Surg 32, 977–987.

Damiano, E.R., Long, D.S., Smith, M.L., 2004. Estimation of viscosity profiles using velocimetry data from parallel flows of linearly viscous fluids: application to microvascular haemodynamics. J Fluid Mech 512, 1–19.

Daniell, M.D., Hill, J.S., 1991. A history of photodynamic therapy. Aust NZ J Surg 61, 340–348.

Das, B., Johnson, P.C., Popel, A.S., 1998. Effect of non-axisymmetric hematocrit distribution on non-Newtonian blood flow in small tubes. Biorheology 35, 69–87.

Das, B., Bishop, J.J., Kim, S., Meiselman, H.J., Johnson, P.C., Popel, A.S., 2007. Red blood cell velocity profiles in skeletal muscle venules at low flow rates are described by the Casson model. Clinical Hemorheology and Microcirculation 36, 217–233.

Detty, M.R., Gibson, S.L., Wagner, S.J., 2004. Current clinical and preclinical photosensitizers for use in photodynamic therapy. J Med Chem 47, 3897–3915.

Dolmans, D.E., Fukumura, D., Jain, R.K., 2003. Photodynamic therapy for cancer. Nat Rev Cancer 3, 380–387.

Dolmans, D.E., Kadambi, A., Hill, J.S., Waters, C.A., Robinson, B.C., Walker, J.P., Fukumura, D., Jain, R.K., 2002. Vascular accumulation of a novel photosensitizer, MV6401, causes selective thrombosis in tumor vessels after photodynamic therapy. Cancer Res 62, 2151–2156.

Dougherty, T.J., 2002. An update on photodynamic therapy applications. J Clin Laser Med Surg 20, 3–7.

Dougherty, T.J., Gomer, C.J., Henderson, B.W., Jori, G., Kessel, D., Korbelik, M., Moan, J., Peng, Q., 1998. Photodynamic therapy. J Natl Cancer Inst 90, 889–905.

Fingar, V.H., Kik, P.K., Haydon, P.S., Cerrito, P.B., Tseng, M., Abang, E., Wieman, T.J., 1999. Analysis of acute vascular damage after photodynamic therapy using benzoporphyrin derivative (BPD). Br J Cancer 79, 1702–1708.

Fu, B.M., Adamson, R.H., Curry, F.E., 1998. Test of two pathway model for small solute exchange across the capillary wall. Am J Physiol 274, H2062–H2073.

Fu, B.M., Shen, S., 2003. Structural mechanisms of acute VEGF effect on microvessel permeability. Am J Physiol Heart Circ Physiol. 284, H2124–35.

Fu, B.M., Shen, S., 2004. Acute VEGF effect on solute permeability of mammalian microvessels in vivo. Microvasc Res 68, 51–62.

Fu, B.M., Tsay, R., Curry, F.E., Weinbaum, S., 1994. A Junction-orifice-fiber entrance layer model for capillary permeability: application to frog mesenteric capillaries. J. Biomech Eng 116, 502–513.

Fungaloi, P., Waterman, P., Nigri, G., Statius-van Eps R., Sluiter, W., van Urk, H., LaMuraglia, G., 2003. Photochemically modulated endothelial cell thrombogenicity via the thrombomodulin-tissue factor pathways. Photochem Photobiol 78, 475–480.

Gaugler, M.H., Squiban, C., Van der Meeren, A., Bertho, J.M., Vandamme, M., Mouthon, M.A., 1997. Late and persistent up-regulation of intercellular adhesion molecule-1 (ICAM-1) expression by ionizing radiation in human endothelial cells in vitro. Int J Radiat Biol 72, 201–209.

Grabowski, E.F., 1995. Thrombolysis, flow and vessel wall interactions. J Vasc Interv Radiol 6, 25S–29S.

Guo, P., Weinstein, A.M., Weinbaum, S., 2000. A hydrodynamic mechanosensory hypothesis for bursh border microvilli. Am J Physiol Renal Physiol 279, F698–F712.

Hallahan, D.E., Virudachalam S., 1999. Accumulation of P-selectin in the lumen of irradiated blood vessels. Radiat Res 152, 6–13.

He, P., Zeng, M., Curry, F.E., 1998. cGMP modulates basal and activated microvessel permeability independent of [Ca2+]i. Am J Physiol: Heart Circ Physiol 274, H1865–H1874.

Holme, P.A., Ørvim, U., Hamers, M.J., Solum, N.O., Brosstad, F.R., Barstad, R.M., Sakariassen, K.S., 1997. Shear-induced platelet activation and platelet microparticle

formation at blood flow conditions as in arteries with a severe stenosis. Arterioscler, Thromb, Vasc Biol 17, 646–653.

Hume, M., Sevitt, S., Thomas, D.P., 1970. Mechanisms of venous thromboembolism. In: Hume, M., Sevitt, S., Thomas, D.P. (Eds.), Venous Thrombosis and Pulmonary Embolism. Harvard University Press, Cambridge, MA, pp. 85–114.

Kendall, S., Michel, C.C., 1995. The measurement of permeability in single rat venules using the red cell microperfusion technique. Exp Physiol. 80, 359–72.

Kübler, A.C., Stenzel, W., Rühling, M., Meul, B., Fischer, J.H., 2003. Experimental evaluation of possible side effects of intra-operative photodynamic therapy on rabbit blood vessels and nerves. Lasers Surg Med 33, 247–255.

Kumagai, R., Lu, X., Kassab, G.S., 2009. Role of glycocalyx in flow-induced production of nitric oxide and reactive oxygen species. Free Radic Biol Med 47, 600–607.

Leunig, M., Leunig, A., Lankes, P., Goeta, A.E., 1994. Evaluation of photodynamic therapy-induced heating of hamster melanoma and its effect on local tumour eradication. Int J Hyperthermia, 10, 297–306.

Levenson, J., Flaud, P., Pino, M.D., Simon, A., 1990. Blood viscosity as a chronic contributing factor of vasodilatation in humans. J Hypertens 8, 1049–1055.

Lipowsky, H.H., Usami, S., Chien, S., 1980. In vivo measurements of ‘‘apparent viscosity’’ and microvessel hematocrit in the mesentery of the cat. Microvasc Res 19 (3), 297–319.

Massad, L., Plotkine, M., Capdeville, C., Boulu, R.G., 1987. Electrically induced arterial thrombosis model in the conscious rat. Thromb Res 48, 1–10.

Merrill, E.W., Margetts, W.G., Cokelet, G.R., Gilliland, E.W., 1963. The Casson equation and rheology of blood near zero shear. In: Copley, A. (Ed.), Symposium on Biorheology. Interscience Pubishers, New York, pp. 135–143.

Michel, C.C., Curry, F.E., 1999. Microvascular permeability. Physiol Rev 79:703-761

Michels, S., Schmidt-Erfurth, U., 2003.Sequence of early vascular events after photodynamic therapy. Invest Ophthalmol Vis Sci 44, 2147–2154.

Most, D., Kozlow, J., Heller, J., Shermak, M.A., 2005. Thromboembolism in plastic surgery. Plast Reconstr Surg 115, 20e–30e.

Mouthon, M.A., Vereycken-Holler, V., Van der Meeren, A., Gaugler, M.H., 2003. Irradiation increases the interactions of platelets with the endothelium in vivo: analysis by intravital microscopy. Radiat Res 160, 593–599.

Muga, K.M., Melton, L.G., Gabriel, D.A., 1995. A flow dynamic technique used to assess global hemostasis. Blood Coag Fibrinol 6, 73–78.

Mulivor, A.W., Lipowsky H.H., 2002. Role of glycocalyx in leukocyte-endothelial cell adhesion. Am J Physiol Heart Circ Physiol 283, H1282–1291.

Nagamine, N., Ido, K., Saihuku, K., Higashizawa, T., Ono, K., Hirasawa, T., Sugano, K., Chong J., 2002. Photodynamic effects on rabbit auricular veins after photosensitization with porfimer sodium: implications of the results with respect to the treatment of esophageal varices with photodynamic therapy. Gastrointest Endosc 55, 420–424.

Nicolaides, A.N., Kakkar, V.V., Field, E.S., Fish, P., 1972. Venous stasis and deep-vein thrombosis. Br J Surg 59, 713–717.

Noren, D., Palmer, H.J., Frame, M.D., 2000. Predicted wall shear rate gradients in Ttype arteriolar bifurcations. Biorheology 37, 325–340.

O'Brien, J.R., 1990. Shear-induced platelet aggregation. Lancet 335, 711–713.

Ortner, M.A., Dorta G., 2006. Technology insight: photodynamic therapy for cholangiocarcinoma. Nat Clin Pract Gastroenterol Hepatol 3, 459–467.

Povlishock, J.T., Rosenblum, W.I., Sholley, M.M., Wei, E.P., 1983. An ultrastructural analysis of endothelial change paralleling platelet aggregation in a light/dye model of microvascular insult. Am J Pathol 110:148–160.

Pries, A.R., Kuebler, W.M., 2006. Normal endothelium. Handb Exp Pharmacol 176, 1–40.

Pries, A.R., Neuhaus, D., Gaehtgens, P., 1992. Blood viscosity in tube flow: dependence on diameter and hematocrit. Am J Physiol: Heart and Circulatory Physiology 263, H1770–H1778.

Pries, A.R., Secomb T.W., Gaehtgens P., 2000. The endothelial surface layer. Pflugers Arch 440, 653–656.

Probst, R.J., Lim, J.M., Bird, D.N., Pole, G.L., Sato, A.K., Claybaugh, J.R., 2006. Gender differences in the blood volume of conscious Sprague-Dawley rats. J Am Assoc Lab Anim Sci 45:49–52.

Proske, S., Vollmar, B., Menger, M.D., 2000. Microvascular consequences of thrombosis in small venules: An in vivo microscopic study using a novel model in the ear of the hairless mouse. Thromb Res 98, 491–498.

Reed, M.W., Miller, F.N., 1988. Importance of light dose in fluorescent microscopy. Microvasc Res 36, 104–107.

Reed, M.W., Wieman, T.J., Schuschke, D.A., Tseng, M.T., Miller, F.N., 1989. A comparison of the effects of photodynamic therapy on normal and tumor blood vessels in the rat microcirculation. Radiat Res 119, 542–552.

Reinhart, W.H., 1994. Shear-dependence of endothelial functions. Experientia 50, 87–93.

Reinisch, J.F., Bresnick, M.D., Walker, J.W., Rosso, R.F., 2001. Deep venous thrombosis and pulmonary embolus after face lift: a study of incidence and prophylaxis. Plast Reconstr Surg 107, 1570–1575.

Reitsma, S., Slaaf, D.W., Vink, H., van Zandvoort, M.A., oude Egbrink, M.G., 2007. The endothelial glycocalyx: composition, functions, and visualization. Pflugers Arch 454, 345–359.

Rosenblum, W.I., El-Sabban, F., 1977. Platelet aggregation in the cerebral microcirculation: effect of aspirin and other agents. Circ Res 40, 320–328.

Rucker, M., Schafer, T., Stamm, A., Saueressig, K., Vollmar, B., Spitzer, W.J., Menger, M.D., 2002. New model for in vivo quantification of microvascular embolization, thrombus formation and recanalization in composite flaps. J Surg Res 108, 129–137.

Rumbaut, R.E., Randhawa, J.K., Smith, C.W., Burns, A.R., 2004. Mouse cremaster venules are predisposed to light/dye-induced thrombosis independent of wall shear rate, CD18, ICAM-1, or P-selectin. Microcirculation 11, 229–247.

Rumbaut, R.E., Slaaf, D.W., Burns, A.R., 2005. Microvascular thrombosis models in venules and arterioles in vivo. Microcirculation 12, 259–274.

Sasaki, T., Kuzuya, M., Cheng, X.W., Nakamura, K., Tamaya-Mori, N., Madea, K., Kanda, S., Koike, T., Sato, K., Iguchi, A., 2004. A novel model of occlusive thrombus formation in mice. Lab Invest 84, 1526–1532.

Sato, M., Ohshima, N., 1984. Platelet thrombus induced in vivo by filtered light and fluorescent dye in mesenteric microvessels of the rat. Thromb Res 35, 319–334.

Sato, M., Ohshima, N., 1990. Effect of wall shear rate on thrombogenesis in microvessels of the rat mesentery. Circ Res 66, 941–949.

Seiffge, D., Kremer, E., 1986. Influence of ADP, blood flow velocity and vessel diameter on the laser-induced thrombus formation. Thromb Res 42, 331–341.

Smith, M.L., Long, D.S., Damiano, E.R., Ley, K., 2003. Near-wall μ-PIV reveals a hydrodynamically relevant endothelial surface layer in venules in vivo. Biophys J 85, 637-645.

Squire, J.M., Chew, M., Nneji, G., Neal, C., Barry, J., Michel, C., 2001. Quasi-periodic substructure in the microvessel endothelial glycocalyx: a possible explanation for molecular filtering? J Struct Biol 136, 239–255.

Sugihara-Seki, M., Fu, B.M., 2005. Blood flow and permeability in microvessels. Fluid Dyna Res 37, 82-132.

Tailor, A., Cooper, D., Granger, D.N., 2005. Platelet-vessel wall interactions in the microcirculation. Microcirculation 12, 275-285.

Tangelder, G.J., Teirlinck, H.C., Slaaf, D.W., Reneman, R.S., 1985. Distribution of blood platelets flowing in arterioles. Am J Physiol: Heart and Circulatory Physiol 248, H318–H323.

Thorlacius, H., Vollmar, B., Seyfert, U.T., Vestweber, D., Menger, M.D., 2000. The polysaccharide fucoidan inhibits microvascular thrombus formation independently from P- and L-selectin function in vivo. Eur J Clin Invest 30, 804-810.

Turitto, V., Hall, C., 1998. Mechanical factors affecting hemostasis and thrombosis. Thrombosis Res 92 (6 Suppl 2), S25–S31.

Valenzeno, D.P., 1987. Photomodification of biological membranes with emphasis on singlet oxygen mechanisms. Photochem Photobiol 46, 147-160.

Valenzeno, D.P., Pooler, J.P, 1982. Cell membrane photomodification: relative effectiveness of halogenated fluoresceins for photohemolysis. Photochem Photobiol 35, 343-350.

Vincent, P.E., Sherwin, S.J., Weinberg, P.D., 2008 Viscous flow over outflow slits covered by an anisotropic Brinkman medium: A model of flow above interendothelial cell clefts. Phys Fluids 20, 063106-1– 063106-11.

Vink, H., Duling, B.R., 1996. Identification of distinct luminal domains for macromolecules, erythrocytes, and leukocytes within mammalian capillaries. Circ Res 79, 581-589.

Weinbaum, S., Tarbell, J.M., Damiano, E.R., 2007. The structure and function of the endothelial glycocalyx layer. Annu Rev Biomed Eng 9, 121-167.

Weinbaum, S., Zhang, X., Han, Y., Vink, H., Cowin, S.C., 2003. Mechano-transduction and flow across the endothelial glycocalyx. PNAS 100, 7988-7995.

Wessler, S., 1962. Thrombosis in the presence of vascular stasis. Am J Med 33, 648–666.

White, F.M., 1962. Laminar flow in a uniformly porous tube. J Appl Mech 29, 201-204.

White, F.M., Barfield, B.F., Goglia, M.J., 1958. Laminar flow in a uniformly porous channel. J Appl Mech 25, 613-617.

Wong, P.C., Crain, E.J., Knabb, R.M., Meade, R.P., Quan, M.L., Watson, C.A., Wexler, R.R., Wright, M.R., Slee, A.M., 2000. Nonpeptide factor Xa inhibitors II. Antithrombotic evaluation in a rabbit model of electrically induced carotid artery thrombosis. J Pharmacol Exp Ther 295, 212–218.

Wootton, D.M., Ku, D.N., 1999. Fluid mechanics of vascular systems, diseases, and thrombosis. Annu Rev Biomed Eng 1, 299–329.

Yuan, W., Lv, Y., Zeng, M., Fu, B.M., 2009. Non-invasive measurement of solute permeability in cerebral microvessels of the rat. Microvasc Res 77:166-173.